

**UNIVERSITI PUTRA MALAYSIA**

***PREPARATION AND ELECTRICAL  
PROPERTIES OF BISMUTH TUNGSTATE  
SOLID ELECTROLYTES***

**YUEN MEI LIAN**

**FS 2016 13**



**PREPARATION AND ELECTRICAL  
PROPERTIES OF BISMUTH TUNGSTATE  
SOLID ELECTROLYTES**

**By**

**YUEN MEI LIAN**

**Thesis Submitted to the School of Graduate Studies, Universiti Putra Malaysia, in  
Fulfilment of the Requirements for the Degree of Doctor of Philosophy**

**February 2016**

All material contained within the thesis, including without limitation text, logos, icons, photographs and all other artwork, is copyright material of Universiti Putra Malaysia unless otherwise stated. Use may be made of any material contained within the thesis for non-commercial purposes from the copyright holder. Commercial use of material may only be made with the express, prior, written permission of Universiti Putra Malaysia.

Copyright © Universiti Putra Malaysia



Abstract of thesis presented to the Senate of Universiti Putra Malaysia in fulfilment of the requirement for the degree of Doctor of Philosophy

## PREPARATION AND ELECTRICAL PROPERTIES OF BISMUTH TUNGSTATE SOLID ELECTROLYTES

By

YUEN MEI LIAN

February 2016

Chairman: Tan Yen Ping, PhD

Faculty: Science

Solid oxide fuel cells (SOFCs) are high efficiency power generators and operated at high temperature (1000 °C). Consequently, this high operating temperature may lead to many technological problems, such as material durability. Bismuth based electrolytes are able to perform higher ion conductivity than the current electrolytes (zirconia based) due to its intrinsic property (a quarter of oxygen sites for ions mobility). However,  $\delta$ -Bi<sub>2</sub>O<sub>3</sub> can exhibit high oxide ion conductivity at limited temperature range (730 °C to 825 °C). Introduction of WO<sub>3</sub> into Bi<sub>2</sub>O<sub>3</sub> was conducted in an attempt to stabilize  $\delta$ -Bi<sub>2</sub>O<sub>3</sub> down to room temperature. Unfortunately, the produced WO<sub>3</sub> doped Bi<sub>2</sub>O<sub>3</sub> materials with a general formula of (1-x)Bi<sub>2</sub>O<sub>3</sub>-xWO<sub>3</sub>, (0.22 ≤ x ≤ 0.255), were unable to stabilize  $\delta$ -Bi<sub>2</sub>O<sub>3</sub>. Eventually, these materials synthesized via conventional solid state method and mechanochemical method, respectively, were fully indexed on the tetragonal system with space group *I41*. Single phase material of Bi<sub>6.24</sub>W<sub>0.88</sub>O<sub>12</sub>, can be obtained at lower temperature with shorter durations through mechanochemical method. The tetragonal structure, Bi<sub>6.24</sub>W<sub>0.88</sub>O<sub>12</sub>, synthesised through mechanochemical method was obtained at 650 °C for 24 hours, while the conventional solid state method synthesized material required a higher temperature (700 °C) for longer duration (48 hours) to obtain a pure phase material.

It must be highlighted that Bi<sub>6.24</sub>W<sub>0.88</sub>O<sub>12</sub> did not undergo decomposition under the studied temperature range (room temperature to 910 °C) based on the XRD patterns from thermal stability experiment and data from thermogravimetric analysis (TGA). This behavior clearly indicated that Bi<sub>6.24</sub>W<sub>0.88</sub>O<sub>12</sub> was a high stability material. Three vibration bands ( $\nu$ (W-O-W), Bi-O and  $\nu$ (W-O)) were noticed in spectra of Fourier-transform infrared (FT-IR) spectroscopy. Scanning Electron Microscopy (SEM) micrographs for pellets sintered at 900 °C illustrated greater grain size compared to pellets sintered at 700 °C. It was inferred that resistance of material could be reduced. X-ray Fluorescence (XRF) analysis recorded data with percentage of error below 5 %,

hence, this validated that compositions material and gave a confidence of the current work results.

$\text{Bi}_{6.24}\text{W}_{0.88}\text{O}_{12}$  exhibited the best ionic conductivity among other solid solutions of  $(1-x)\text{Bi}_2\text{O}_3-x\text{WO}_3$ , ( $0.22 \leq x \leq 0.255$ ).  $\text{Bi}_{6.24}\text{W}_{0.88}\text{O}_{12}$  fabricated by mechanochemical method demonstrated the highest conductivity of  $2.25 \times 10^{-2} \text{ ohm}^{-1}\text{cm}^{-1}$  at  $600 \text{ }^\circ\text{C}$  (average grain size of  $12.46 \text{ }\mu\text{m}$  to  $48.16 \text{ }\mu\text{m}$ ) than conventional solid state route materials. It was also worthwhile to point out that a pure  $\text{Bi}_{6.24}\text{W}_{0.88}\text{O}_{12}$  ion conducting solid electrolyte without any electronic conduction was produced with ionic conductivity of 6 orders higher than the reported YSZ at  $600 \text{ }^\circ\text{C}$ , elucidating a greater potential of  $\text{Bi}_{6.24}\text{W}_{0.88}\text{O}_{12}$  to be used as a material utilized in SOFC electrolytes applications.

Doping was carried out on the Bi or W sites in  $\text{Bi}_{6.24}\text{W}_{0.88}\text{O}_{12}$  with selected dopants, including monovalent ( $\text{Li}^+$ ), divalent ( $\text{Ca}^{2+}$ ,  $\text{Cu}^{2+}$ ,  $\text{Ni}^{2+}$  and  $\text{Zn}^{2+}$ ), trivalent ( $\text{Cr}^{3+}$  and  $\text{Y}^{3+}$ ), tetravalent ( $\text{Sn}^{4+}$ ,  $\text{Ti}^{4+}$  and  $\text{Zr}^{4+}$ ), pentavalent ( $\text{Sb}^{5+}$ ,  $\text{V}^{5+}$ ,  $\text{Nb}^{5+}$  and  $\text{Ta}^{5+}$ ) and hexavalent ( $\text{Mo}^{6+}$ ) cations in order to investigate their effects on the electrical properties of doped  $\text{Bi}_{6.24}\text{W}_{0.88}\text{O}_{12}$  materials. All these dopants can be introduced into  $\text{Bi}_{6.24}\text{W}_{0.88}\text{O}_{12}$  with rather limited solid solution ranges. Ion vacancy, ionic potential and unit cell parameters of structure are the main factors that varying the conductivity of the doped materials.  $\text{Bi}_{6.24}\text{W}_{0.68}\text{Nb}_{0.20}\text{O}_{11.900}$  was developed and achieved the highest oxide ion conductivity ( $2.96 \times 10^{-2} \text{ ohm}^{-1}\text{cm}^{-1}$  at  $600 \text{ }^\circ\text{C}$ ) among other cation dopants. This doped material was 32 % more conductive than the undoped material. Therefore, it is important to point that this doped material could elevated the performance of SOFC. Nb particles (tiny particle) were homogeneously distributed over the surface ceramic of  $\text{Bi}_{6.24}\text{W}_{0.68}\text{Nb}_{0.20}\text{O}_{11.900}$  as illustrated in SEM image.

Abstrak tesis yang dikemukakan kepada Senat Universiti Putra Malaysia sebagai memenuhi keperluan untuk ijazah Doktor Falsafah

**PENYEDIAAN DAN SIFAT ELEKTRIK BISMUT  
TUNGSTAN ELEKTROLIT PEPEJAL**

Oleh

**YUEN MEI LIAN**

**Februari 2016**

**Pengerusi: Tan Yen Ping, PhD**

**Fakulti: Sains**

Sel bahan api pepejal oksida (SOFC) ialah penjana kuasa yang berkecekapan tinggi dan beroperasi pada suhu tinggi (1000 °C). Akibatnya, suhu operasi yang tinggi ini membawa banyak masalah teknologi, contohnya ketahanan bahan. Elektrolit berdasarkan bismut boleh melaksanakan kekonduksian ion yang lebih baik daripada elektrolit semasa (berdasarkan zirkonia) disebabkan oleh sifat intrinsiknya (satu suku ruang oksigen untuk pergerakan ion). Namun demikian,  $\delta$ -Bi<sub>2</sub>O<sub>3</sub> dapat menunjukkan kekonduksian ion yang tinggi pada julat suhu terhad (730 °C ke 825 °C). Pengaliran WO<sub>3</sub> ke dalam Bi<sub>2</sub>O<sub>3</sub> dilakukan dengan tujuan untuk menstabilkan  $\delta$ -Bi<sub>2</sub>O<sub>3</sub> hingga ke suhu bilik. Malangnya, bahan WO<sub>3</sub> terdop Bi<sub>2</sub>O<sub>3</sub> dengan formula umum (1-x)Bi<sub>2</sub>O<sub>3</sub>-xWO<sub>3</sub>, (0.22 ≤ x ≤ 0.255), yang terhasil ini gagal menstabilkan  $\delta$ -Bi<sub>2</sub>O<sub>3</sub>. Akhirnya, bahan tersebut yang disintesis dengan tindak balas keadaan pepejal secara konvensional dan mekanokimia secara berasingan, dapat diindekskan pada sistem tetragonal dengan kumpulan ruang *I41*. Bahan berfasa tunggal bagi Bi<sub>6.24</sub>W<sub>0.88</sub>O<sub>12</sub>, boleh diperolehi pada suhu yang lebih rendah dengan masa yang lebih singkat yang disintesis melalui tindak balas mekanokimia. Struktur tetragonal, Bi<sub>6.24</sub>W<sub>0.88</sub>O<sub>12</sub>, yang disintesis melalui tindak balas mekanokimia dapat diperolehi pada 650 °C selama 24 jam, manakala bahan bagi tindak balas keadaan pepejal secara konvensional memerlukan lebih tinggi suhu (700 °C) dengan lebih panjang tempoh (48 jam) untuk mendapatkan bahan berfasa tunggal.

Dengan ini, dapat menegaskan bahawa Bi<sub>6.24</sub>W<sub>0.88</sub>O<sub>12</sub> tidak mengalami sebarang penguraian di bawah julat suhu yang dikaji (suhu bilik ke 910 °C) berdasarkan corak XRD daripada eksperimen kestabilan haba dan data daripada from analisis termogravimetri (TGA). Sifat ini jelas menunjukkan bahawa Bi<sub>6.24</sub>W<sub>0.88</sub>O<sub>12</sub> adalah bahan yang berkestabilan tinggi. Tiga jalur getaran ( $\nu$ (W-O-W), Bi-O and  $\nu$ (W-O)) dapat diperhatikan dalam spektra spektroskopi inframerah transformasi Fourier (FT-IR). Mikrograf imbasan elektron mikroskopi (SEM) bagi pelet disinter pada suhu 900 °C mempamerkan butiran yang bersaiz besar berbanding dengan pelet disinter pada

suhu 700 °C. Ini boleh dikatakan rintangan bahan dapat dikurangkan. Analisis pendarfluor X-ray (XRF) mencatat data dengan peratusan ralat di bawah 5 %, jadi, ini mengesahkan bahan komposisi dan memberikan satu keyakinan terhadap keputusan kerja ini.

$\text{Bi}_{6.24}\text{W}_{0.88}\text{O}_{12}$  mempamerkan kekonduksian ionik terbaik di kalangan larutan pepejal bagi  $(1-x)\text{Bi}_2\text{O}_3-x\text{WO}_3$ , ( $0.22 \leq x \leq 0.255$ ).  $\text{Bi}_{6.24}\text{W}_{0.88}\text{O}_{12}$  yang diperbuat melalui tindak balas mekanokimia menunjukkan kekonduksian paling tinggi dengan  $2.25 \times 10^{-2} \text{ ohm}^{-1}\text{cm}^{-1}$  pada 600 °C (saiz purata bijirin adalah 12.46  $\mu\text{m}$  ke 48.16  $\mu\text{m}$ ) daripada bahan tindak balas keadaan pepejal secara konvensional. Dengan ini adalah berbaloi menunjukkan  $\text{Bi}_{6.24}\text{W}_{0.88}\text{O}_{12}$  elektrolit pepejal ionik tulen tanpa kekonduksian elektronik dihasilkan dengan konduksi ionik sebanyak 6 kali lebih tinggi daripada YSZ yang dilaporkan pada 600 °C, menjelaskan  $\text{Bi}_{6.24}\text{W}_{0.88}\text{O}_{12}$  berpotensi agung apabila bahan ini digunakan dalam SOFC sebagai elektrolit.

Pendopan dijalankan pada tapak Bi atau W bagi  $\text{Bi}_{6.24}\text{W}_{0.88}\text{O}_{12}$  dengan dopan yang terpilih, termasuk kation monovalen ( $\text{Li}^+$ ), divalen ( $\text{Ca}^{2+}$ ,  $\text{Cu}^{2+}$ ,  $\text{Ni}^{2+}$  and  $\text{Zn}^{2+}$ ), trivalen ( $\text{Cr}^{3+}$  and  $\text{Y}^{3+}$ ), tetravalen ( $\text{Sn}^{4+}$ ,  $\text{Ti}^{4+}$  and  $\text{Zr}^{4+}$ ), pentavalen ( $\text{Sb}^{5+}$ ,  $\text{V}^{5+}$ ,  $\text{Nb}^{5+}$  and  $\text{Ta}^{5+}$ ) and heksavalen ( $\text{Mo}^{6+}$ ) bagi mengkaji kesan pendopan pada sifat elektrik pada bahan terdop  $\text{Bi}_{6.24}\text{W}_{0.88}\text{O}_{12}$ . Semua dopan yang diperkenalkan ke dalam  $\text{Bi}_{6.24}\text{W}_{0.88}\text{O}_{12}$  mempunyai julat larutan pepejal terhad. Kekosongan ion, keupayaan ionik dan parameter sel unit struktur merupakan faktor utama yang mempengaruhi kekonduksian bagi bahan terdop.  $\text{Bi}_{6.24}\text{W}_{0.68}\text{Nb}_{0.20}\text{O}_{11.900}$  dihasilkan dan mencapai kekonduksian ion yang tertinggi ( $2.96 \times 10^{-2} \text{ ohm}^{-1} \text{ cm}^{-1}$  pada 600 °C) di kalangan bahan dopan kation. Bahan terdop ini adalah 32 % lebih mengkonduksi daripada bahan tidak terdop. Oleh itu, ini adalah penting mengatakan bahawa bahan terdop ini boleh menaikkan prestasi SOFC. Zarah Nb (zarah kecil) adalah bertaburan secara homogen pada permukaan seramik seperti yang digambarkan di imej SEM.

## ACKNOWLEDGEMENTS

First of all, I would like to express my deepest gratitude and truly appreciation to my project supervisor, Dr. Tan Yen Ping for her dedication, invaluable guidance, constructive comments, continuous support, patience, innovative ideas and concern throughout the duration of this study. I extend my sincere appreciation to Dr. Tan Kar Ban and Prof. Dr. Taufiq Yap Yun Hin for their advice and suggestion throughout the completion of my study.

In addition, I would also like to thank staff from the Microscopy and Microanalysis Unit, Enzyme and Microbe Technology Laboratory, Nanoscience Strategic Unit, Institute of Bioscience, UPM for helping me to run SEM analysis and interpreting the data. Besides that, a deep acknowledgement is also extended to the lecturer and staff of the Department of Chemistry, Universiti Putra Malaysia for the provision of laboratory facilities. Sincere thanks attributed to all my friends and labmates in Chemistry Laboratory 128 for their kindness and willingness in guiding and helping me throughout my study.

To my beloved parents and family, I would like to express my deepest affection for their consistent support, endless love, encouragement and understanding towards the completion of this study.

Finally, scholarship award from University Malaysia Pahang under the Ministry of Higher Education and staff are gratefully acknowledged. Without them, it would not have been possible for me to go this far.

I certify that a Thesis Examination Committee has met on 23 February 2016 to conduct the final examination of Yuen Mei Lian on her thesis entitled "Preparation and Electrical Properties of Bismuth Tungstate Solid Electrolytes" in accordance with the Universities and University Colleges Act 1971 and the Constitution of the Universiti Putra Malaysia [P.U.(A) 106] 15 March 1998. The Committee recommends that the student be awarded the Doctor of Philosophy.

Members of the Thesis Examination Committee were as follows:

**Gwendoline Ee Cheng Lian, PhD**

Professor  
Faculty of Science  
Universiti Putra Malaysia  
(Chairman)

**Halimah binti Mohamed Kamari, PhD**

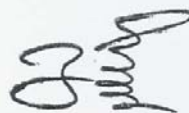
Associate Professor  
Faculty of Science  
Universiti Putra Malaysia  
(Internal Examiner)

**Mohd Zaizi bin Desa, PhD**

Associate Professor  
Faculty of Science  
Universiti Putra Malaysia  
(Internal Examiner)

**Tseung-Yuen Tseng, PhD**

Professor  
National Chiao Tung University  
Taiwan  
(External Examiner)



---

**ZULKARNAIN ZAINAL, PhD**

Professor and Deputy Dean  
School of Graduate Studies  
Universiti Putra Malaysia

Date: 21 April 2016

This thesis was submitted to the Senate of Universiti Putra Malaysia and has been accepted as fulfilment of the requirement for the degree of Doctor of Philosophy. The members of the Supervisory Committee were as follows:

**Tan Yen Ping, PhD**

Senior Lecturer  
Faculty of Science  
Universiti Putra Malaysia  
(Chairman)

**Taufiq Yap Yun Hin, PhD**

Professor  
Faculty of Science  
Universiti Putra Malaysia  
(Member)

**Tan Kar Ban, PhD**

Senior Lecturer  
Faculty of Science  
Universiti Putra Malaysia  
(Member)

**BUJANG KIM HUAT, PhD**

Professor and Dean  
School of Graduate Studies  
Universiti Putra Malaysia

Date:

### **Declaration by graduate student**

I hereby confirm that:

- this thesis is my original work;
- quotations, illustrations and citations have been duly referenced;
- this thesis has not been submitted previously or concurrently for any other degree at any other institutions;
- intellectual property from the thesis and copyright of thesis are fully-owned by Universiti Putra Malaysia, as according to the Universiti Putra Malaysia (Research) Rules 2012;
- written permission must be obtained from supervisor and the office of Deputy Vice-Chancellor (Research and Innovation) before thesis is published (in the form of written, printed or in electronic form) including books, journals, modules, proceedings, popular writings, seminar papers, manuscripts, posters, reports, lecture notes, learning modules or any other materials as stated in the Universiti Putra Malaysia (Research) Rules 2012;
- there is no plagiarism or data falsification/fabrication in the thesis, and scholarly integrity is upheld as according to the Universiti Putra Malaysia (Graduate Studies) Rules 2003 (Revision 2012-2013) and the Universiti Putra Malaysia (Research) Rules 2012. The thesis has undergone plagiarism detection software.

Signature: \_\_\_\_\_ Date: \_\_\_\_\_

Name and Matric No.: Yuen Mei Lian, GS26849

### **Declaration by Members of Supervisory Committee**

This is to confirm that:

- the research conducted and the writing of this thesis was under our supervision;
- supervision responsibilities as stated in the Universiti Putra Malaysia (Graduate Studies) Rules 2003 (Revision 2012-2013) are adhered to.

Signature: \_\_\_\_\_  
Name of Chairman of Supervisory Committee: Tan Yen Ping, PhD

Signature: \_\_\_\_\_  
Name of Member of Supervisory Committee: Taufiq Yap Yun Hin, PhD

Signature: \_\_\_\_\_  
Name of Member of Supervisory Committee: Tan Kar Ban, PhD

## TABLE OF CONTENTS

		<b>Page</b>
<b>ABSTRACT</b>		i
<b>ABSTRAK</b>		iii
<b>ACKNOWLEDGEMENTS</b>		v
<b>APPROVAL</b>		vi
<b>DECLARATION</b>		viii
<b>LIST OF TABLES</b>		xii
<b>LIST OF FIGURES</b>		xv
<b>LIST OF ABBREVIATIONS</b>		xxv
 <b>CHAPTER</b>		
<b>1</b>	<b>INTRODUCTION</b>	<b>1</b>
	1.1 Electroceramics	1
	1.2 Solid Oxide Electrolyte	2
	1.2.1 Overview	2
	1.2.2 Conduction Mechanism	3
	1.2.3 Application	5
	1.2.3.1 Solid Oxide Fuel Cells (SOFC)	5
	1.2.3.2 Oxygen Sensor	7
	1.3 Solid Solutions	8
	1.4 Problem Statements	10
	1.5 Objectives	11
<b>2</b>	<b>LITERATURE REVIEW</b>	<b>12</b>
	2.1 Oxide Ion Conductors	12
	Bi <sub>2</sub> O <sub>3</sub> Oxide Ion Conductor	14
	Metal Cations Doped Bismuth Oxide	17
	Bismuth Tungstate	21
	2.4.1 Metal Cations Doped Bismuth Tungstate	25
<b>3</b>	<b>METHODOLOGY</b>	<b>27</b>
	3.1 Sample Preparation	27
	3.1.1 Conventional Solid State Method	27
	3.1.2 Mechanochemical Method	27
	3.1.3 Chemical Doping	30
	3.2 Pellet Preparation	30
	3.3 Characterization	32
	3.3.1 X-ray Diffraction	32
	3.3.2 Thermogravimetry Analysis	34
	3.3.3 Fourier-Transform Infrared Spectroscopy	34
	3.3.4 Scanning Electron Microscopy	35
	3.3.5 X-ray Fluorescence Spectroscopy	35
	3.4 Electrical Properties	36
	3.4.1 General Principles of AC Method	37
	3.4.2 Cole-cole Plot	38
	3.4.3 Electric Modulus Spectroscopy	43
	3.4.4 Experimental Procedure for Electrical Conductivity Measurement	44

<b>4</b>	<b>RESULTS AND DISCUSSION</b>	<b>46</b>
4.1	Phase Formation	46
4.1.1	Conventional Solid State Method	46
4.1.1.1	Parent Compound, $\text{Bi}_{6.24}\text{W}_{0.88}\text{O}_{12}$	46
4.1.1.2	$(1-x)\text{Bi}_2\text{O}_3-x\text{WO}_3$ , ( $0.22 \leq x \leq 0.255$ ), solid solutions	48
4.2.1	Mechanochemical Method	52
4.1.2.1	Parent Compound, $\text{Bi}_{6.24}\text{W}_{0.88}\text{O}_{12}$	52
4.1.2.2	$(1-x)\text{Bi}_2\text{O}_3-x\text{WO}_3$ , ( $0.22 \leq x \leq 0.255$ ), solid solutions	54
4.2	Thermogravimetry Analysis	59
4.3	Fourier-transform Infrared Spectroscopy	60
4.3.1	$(1-x)\text{Bi}_2\text{O}_3-x\text{WO}_3$ , ( $0.22 \leq x \leq 0.255$ ), Prepared by Conventional Solid State Method	60
4.3.2	$(1-x)\text{Bi}_2\text{O}_3-x\text{WO}_3$ , ( $0.22 \leq x \leq 0.255$ ), Prepared by Mechanochemical Method	62
4.4	Scanning Electron Microscopy	64
4.4.1	$(1-x)\text{Bi}_2\text{O}_3-x\text{WO}_3$ , ( $0.22 \leq x \leq 0.255$ ), Prepared by Conventional Solid State Method	64
4.4.2	$(1-x)\text{Bi}_2\text{O}_3-x\text{WO}_3$ , ( $0.22 \leq x \leq 0.255$ ), Prepared by Mechanochemical Method	70
4.5	X-ray Fluorescence Spectroscopy	79
4.6	Electrical Properties	81
4.6.1	$(1-x)\text{Bi}_2\text{O}_3-x\text{WO}_3$ , ( $0.22 \leq x \leq 0.255$ ), Prepared by Conventional Solid State Method	81
4.6.2	$(1-x)\text{Bi}_2\text{O}_3-x\text{WO}_3$ , ( $0.22 \leq x \leq 0.255$ ), Prepared by Mechanochemical Method	96
4.7	Doped Materials	114
4.7.1	Phase Formation	114
4.7.1.1	Monovalent and Divalent Dopants	114
4.7.1.2	Trivalent and Tetravalent Dopants	119
4.7.1.3	Pentavalent and Hexavalent Dopants	124
4.7.2	Thermogravimetric Analysis	129
4.7.3	Fourier-transform Infrared Spectroscopy	132
4.7.4	Scanning Electron Microscopy	141
4.7.5	Electrical Properties	149
4.7.5.1	Monovalent and Divalent Dopants	149
4.7.5.2	Trivalent and Tetravalent Dopants	156
4.7.5.3	Pentavalent and Hexavalent Dopants	163
<b>5</b>	<b>CONCLUSION AND RECOMMENDATIONS FOR FUTURE RESEARCH</b>	<b>171</b>
5.1	Conclusion	171
5.2	Recommendations for Future Research	172
	<b>REFERENCES</b>	<b>173</b>
	<b>APPENDICES</b>	<b>181</b>
	<b>BIODATA OF STUDENT</b>	<b>187</b>

## LIST OF TABLES

<b>Table</b>		<b>Page</b>
1.1	Examples of electroceramics	2
2.1	Conductivity parameters observed for Bi <sub>2</sub> O <sub>3</sub> phases (Sammes <i>et al.</i> , 1999)	16
3.1	Samples of (1-x)Bi <sub>2</sub> O <sub>3</sub> -xWO <sub>3</sub> , (0.22 ≤ x ≤ 0.255)	27
3.2	List of dopant, purity and company	32
3.3	Capacitance values and their possible interpretation	41
4.1	Phase purity of (1-x)Bi <sub>2</sub> O <sub>3</sub> -xWO <sub>3</sub> , (0.215 ≤ x ≤ 0.260), prepared via conventional solid state method	49
4.2	The lattice parameters of (1-x)Bi <sub>2</sub> O <sub>3</sub> -xWO <sub>3</sub> , (0.22 ≤ x ≤ 0.255), solid solutions from X-ray diffraction data prepared by conventional solid state method	51
4.3	Phase purity of (1-x)Bi <sub>2</sub> O <sub>3</sub> -xWO <sub>3</sub> , (0.215 ≤ x ≤ 0.260), prepared via mechanochemical method (milling rate = 1000 rpm)	55
4.4	Phase purity of Bi <sub>6.24</sub> W <sub>0.88</sub> O <sub>12</sub> , prepared via mechanochemical method, milled at different rates	56
4.5	The lattice parameters of (1-x)Bi <sub>2</sub> O <sub>3</sub> -xWO <sub>3</sub> , (0.22 ≤ x ≤ 0.255), solid solutions from X-ray diffraction data prepared by mechanochemical method (milling rate = 1000 rpm)	58
4.6	Vibration frequencies (cm <sup>-1</sup> ) of (1-x)Bi <sub>2</sub> O <sub>3</sub> -xWO <sub>3</sub> , (0.22 ≤ x ≤ 0.255), prepared via conventional solid state method	62
4.7	Vibration frequencies (cm <sup>-1</sup> ) of (1-x)Bi <sub>2</sub> O <sub>3</sub> -xWO <sub>3</sub> , (0.22 ≤ x ≤ 0.255), prepared via mechanochemical method	63
4.8	Calculated crystallite sizes and grain sizes of (1-x)Bi <sub>2</sub> O <sub>3</sub> -xWO <sub>3</sub> , (0.22 ≤ x ≤ 0.255), prepared by conventional solid state method	78
4.9	Calculated crystallite sizes and grain sizes of (1-x)Bi <sub>2</sub> O <sub>3</sub> -xWO <sub>3</sub> , (0.22 ≤ x ≤ 0.255), prepared by mechanochemical method	78
4.10	XRF analysis of materials in (1-x)Bi <sub>2</sub> O <sub>3</sub> -xWO <sub>3</sub> , (0.22 ≤ x ≤ 0.255), prepared via conventional solid state method	79
4.11	XRF analysis of materials in (1-x)Bi <sub>2</sub> O <sub>3</sub> -xWO <sub>3</sub> , (0.22 ≤ x ≤ 0.255), prepared via mechanochemical method	80
4.12	Conductivities (σ <sub>300</sub> and σ <sub>600</sub> ) and activation energies (E <sub>a</sub> ) of (1-x)Bi <sub>2</sub> O <sub>3</sub> -xWO <sub>3</sub> , (0.22 ≤ x ≤ 0.255), sintered at 700 °C, prepared via	88

	conventional solid state method	
4.13	Conductivities ( $\sigma_{300}$ and $\sigma_{600}$ ) and activation energies ( $E_a$ ) of $(1-x)\text{Bi}_2\text{O}_3-x\text{WO}_3$ , ( $0.22 \leq x \leq 0.255$ ), sintered at 900 °C, prepared via conventional solid state method	88
4.14	Conductivity values at 500 °C and 750 °C for different atmospheres (pellet sintered at 700°C), prepared via conventional solid state method	92
4.15	Conductivity values at 500 °C and 750 °C for different atmospheres (pellet sintered at 900°C), prepared via conventional solid state method	92
4.16	Conductivities ( $\sigma_{300}$ and $\sigma_{600}$ ) and activation energies ( $E_a$ ) of $(1-x)\text{Bi}_2\text{O}_3-x\text{WO}_3$ , ( $0.22 \leq x \leq 0.255$ ), sintered at 700 °C, prepared via mechanochemical method (milling rate = 1000 rpm)	103
4.17	Conductivities ( $\sigma_{300}$ and $\sigma_{600}$ ) and activation energies ( $E_a$ ) of $(1-x)\text{Bi}_2\text{O}_3-x\text{WO}_3$ , ( $0.22 \leq x \leq 0.255$ ), sintered at 900 °C, prepared via mechanochemical method (milling rate = 1000 rpm)	103
4.18	Conductivity values at 500 °C and 750 °C for different atmospheres (pellet sintered at 700 °C), prepared via mechanochemical method (milling rate = 1000 rpm)	106
4.19	Conductivity values at 500°C and 750°C for different atmospheres (pellet sintered at 900 °C), prepared via mechanochemical method (milling rate = 1000 rpm)	106
4.20	The coordination number, charge, atomic mass and ionic radius of metals (Shannon, 1976)	115
4.21	The lattice parameters of monovalent and divalent cations doped into $\text{Bi}_{6.24}\text{W}_{0.88}\text{O}_{12}$	117
4.22	The lattice parameters of trivalent and tetravalent cations doped into $\text{Bi}_{6.24}\text{W}_{0.88}\text{O}_{12}$	122
4.23	The lattice parameters of pentavalent and hexavalent cations doped into $\text{Bi}_{6.24}\text{W}_{0.88}\text{O}_{12}$	126
4.24	Vibrational frequencies ( $\text{cm}^{-1}$ ) of the doped materials	138
4.25	Ionic potential for the various cations substituted into $\text{Bi}_{6.24}\text{W}_{0.88}\text{O}_{12}$	149
4.26	Conductivity ( $\sigma_{300}$ and $\sigma_{600}$ ) and activation energies ( $E_a$ ) of monovalent and divalent doped materials	155
4.27	Conductivity ( $\sigma_{300}$ and $\sigma_{600}$ ) and activation energies ( $E_a$ ) of trivalent and tetravalent doped materials	156

4.28 Conductivity ( $\sigma_{300}$  and  $\sigma_{600}$ ) and activation energies ( $E_a$ ) of 169 pentavalent and hexavalent doped materials



## LIST OF FIGURES

<b>Figure</b>		<b>Page</b>
1.1	Solid electrolytes as intermediate between normal crystalline solids and liquids (West, 1999)	4
1.2	Electrical conductivities of selected common substances and representative solid electrolytes (Greenblatt, 1994)	4
1.3	Schematic of a ceramic fuel cell or solid oxide fuel cell (SOFC) (Huijsmans, 2001)	6
1.4	The operation principle for oxygen sensor (Yamada, T. 2003)	7
2.1	The stable and metastable regions found in $\text{Bi}_2\text{O}_3$ (Shuk <i>et al.</i> , 1996)	13
2.2	Electrical conductivity of $\text{Bi}_2\text{O}_3$ as a function of temperature (Shuk <i>et al.</i> , 1996)	14
2.3	(a) Unit cell of $\delta\text{-Bi}_2\text{O}_3$ (3 bismuth, 4 oxygen, and 2 oxygen vacancy) and (b) Oxygen ionic transport mechanism (Kang <i>et al.</i> , 2013)	14
2.4	Structure models for $\delta\text{-Bi}_2\text{O}_3$ , (a) Sillen model; (b) Gattow model; (c) Willis models (Harwig, 1978)	16
2.5	$\text{Bi}_2\text{O}_3\text{-WO}_3$ system phase diagram (Finlayson <i>et al.</i> , 2005)	20
2.6	Structure of $7\text{Bi}_2\text{O}_3\cdot 2\text{WO}_3$ (Nespolo <i>et al.</i> , 2002) (a) without oxygen atoms (b) with the oxygen atoms	22
2.7	Schematic representation of the relations of the unit-cell axes (Watanabe <i>et al.</i> , 1985)	22
2.8	Unit cell of the tetragonal structure for the present solid solution (Watanabe and Ono, 2004)	23
3.1	Flow chart for sample preparation via conventional solid state method	27
3.2	Flow chart for sample preparation via mechanochemical method	28
3.3	Flow chart for the preparation of metal cation doped $\text{Bi}_{6.24}\text{W}_{0.88}\text{O}_{12}$ via conventional solid state method	30
3.4	Flow chart of sample preparation and characterization route	31
3.5	Admittance bridge (West, 1984)	38
3.6	Semi-circle and spike in a complex plane plot	39
3.7	Possible equivalent circuit for an electric ceramic with bulk and grain	40

	boundary component and its corresponding frequency response in complex plane plots (Ahmadu <i>et al.</i> , 2013)	
3.8	Brickwork model of grain boundary regions in a ceramic placed between metal electrodes (Irvine <i>et al.</i> , 1990)	40
3.9	Equivalent circuit for a polycrystalline solid electrolyte ( $C_{gb}$ , $C_b$ – double-layer capacitance; $C_b$ , $R_b$ – bulk; $C_{gb}$ , $R_{gb}$ – grain boundaries) (Hirose and West, 1996)	42
3.10	Impedance diagram due to a blocking interface: (a) a perfectly smooth interface; (b) rough electrode or due to Warburg impedance (Armstrong and Todd, 1995)	42
3.11	The respective $Z''$ and $M''$ spectroscopic plots (Irvine <i>et al.</i> , 1990)	44
4.1	Phase evolution of $\text{Bi}_{6.24}\text{W}_{0.88}\text{O}_{12}$ synthesized via conventional solid state method at different synthesis temperatures and durations	47
4.2	XRD pattern of $\text{Bi}_{6.24}\text{W}_{0.88}\text{O}_{12}$ prepared by conventional solid state method (heated at 700 °C for 48 hours)	48
4.3	XRD patterns of $(1-x)\text{Bi}_2\text{O}_3-x\text{WO}_3$ , ( $0.215 \leq x \leq 0.260$ ), prepared via solid state method	49
4.4	Variation of lattice parameters, $a=b$ , of solid solutions with $(1-x)\text{Bi}_2\text{O}_3-x\text{WO}_3$ structure, ( $0.22 \leq x \leq 0.255$ ), prepared by conventional solid state method	50
4.5	Variation of lattice parameters, $c$ , of solid solutions with $(1-x)\text{Bi}_2\text{O}_3-x\text{WO}_3$ structure, ( $0.22 \leq x \leq 0.255$ ), prepared by conventional solid state method	50
4.6	Variation of cell volumes, of solid solutions with $(1-x)\text{Bi}_2\text{O}_3-x\text{WO}_3$ structure, ( $0.22 \leq x \leq 0.255$ ), prepared by conventional solid state method	51
4.7	Phase evolution of $\text{Bi}_{6.24}\text{W}_{0.88}\text{O}_{12}$ , synthesized via mechanochemical method at different synthesis temperatures and durations (milling rate = 1000 rpm)	53
4.8	XRD pattern of $\text{Bi}_{6.24}\text{W}_{0.88}\text{O}_{12}$ prepared by mechanochemical method (heated at 650 °C for 24 hours, milling rate = 1000 rpm)	53
4.9	XRD patterns of $(1-x)\text{Bi}_2\text{O}_3-x\text{WO}_3$ , ( $0.215 \leq x \leq 0.26$ ), prepared via mechanochemical method (milling rate = 1000 rpm)	55
4.10	Phase evolution of $\text{Bi}_{6.24}\text{W}_{0.88}\text{O}_{12}$ synthesized via mechanochemical method at different milling rate, synthesis temperatures and durations	56
4.11	Variation of lattice parameters, $a=b$ , of solid solutions with $(1-$	57

	x)Bi <sub>2</sub> O <sub>3</sub> -xWO <sub>3</sub> , (0.22 ≤ x ≤ 0.255), prepared by mechanochemical method (milling rate = 1000 rpm)	
4.12	Variation of lattice parameters, c, of solid solutions with (1-x)Bi <sub>2</sub> O <sub>3</sub> -xWO <sub>3</sub> , (0.22 ≤ x ≤ 0.255), prepared by mechanochemical method (milling rate = 1000 rpm)	57
4.13	Variation of cell volumes of solid solutions with (1-x)Bi <sub>2</sub> O <sub>3</sub> -xWO <sub>3</sub> , (0.22 ≤ x ≤ 0.255), prepared by mechanochemical method (milling rate = 1000 rpm)	58
4.14	TGA thermogram of single phase materials prepared via conventional solid state method from room temperature to 910 °C: (a)Bi <sub>6.24</sub> W <sub>0.88</sub> O <sub>12</sub> ; (b)Bi <sub>6.16</sub> W <sub>0.92</sub> O <sub>12</sub> ; (c)Bi <sub>6.08</sub> W <sub>0.96</sub> O <sub>12</sub> ; (d)Bi <sub>6</sub> WO <sub>12</sub> ; (e)Bi <sub>5.96</sub> W <sub>1.02</sub> O <sub>12</sub>	59
4.15	TGA thermogram of single phase materials prepared via mechanochemical method from room temperature to 910 °C: (a)Bi <sub>6.24</sub> W <sub>0.88</sub> O <sub>12</sub> ; (b)Bi <sub>6.16</sub> W <sub>0.92</sub> O <sub>12</sub> ; (c)Bi <sub>6.08</sub> W <sub>0.96</sub> O <sub>12</sub> ; (d)Bi <sub>6</sub> WO <sub>12</sub> ; (e)Bi <sub>5.96</sub> W <sub>1.02</sub> O <sub>12</sub> ; (f)Bi <sub>6.24</sub> W <sub>0.88</sub> O <sub>12</sub> (milling rate = 700 rpm); (g)Bi <sub>6.24</sub> W <sub>0.88</sub> O <sub>12</sub> (milling rate = 1400 rpm)	60
4.16	IR spectrum of (1-x)Bi <sub>2</sub> O <sub>3</sub> -xWO <sub>3</sub> , (x = 0.220), prepared by conventional solid state method showing (a) the whole spectrum and (b) the far IR region	61
4.17	IR spectra of (1-x)Bi <sub>2</sub> O <sub>3</sub> -xWO <sub>3</sub> , (0.22 ≤ x ≤ 0.255), solid solutions, prepared by conventional solid state method: (a) x=0.220; (b) x=0.230; (c) x=0.240; (d) x=0.250; (e) x=0.255	61
4.18	IR spectrum of (1-x)Bi <sub>2</sub> O <sub>3</sub> -xWO <sub>3</sub> , (x = 0.220) prepared by mechanochemical method (milling rate = 1000 rpm) showing (a) the whole spectrum; (b) the far IR region	62
4.19	IR spectra of (1-x)Bi <sub>2</sub> O <sub>3</sub> -xWO <sub>3</sub> , (0.22 ≤ x ≤ 0.255), prepared by mechanochemical method: (a)x = 0.220; (b)x = 0.230; (c)x = 0.24; (d)x = 0.250; (e)x = 0.255; (f)x = 0.220 (milling rate = 700 rpm); (g)x = 0.220 (milling rate = 1400 rpm)	63
4.20(a)	SEM micrograph of (1-x)Bi <sub>2</sub> O <sub>3</sub> -xWO <sub>3</sub> , x = 0.220, sintered at 700 °C (magnification: 1000x)	65
4.20(b)	SEM micrograph of (1-x)Bi <sub>2</sub> O <sub>3</sub> -xWO <sub>3</sub> , x = 0.230, sintered at 700 °C (magnification: 1000x)	65
4.20(c)	SEM micrograph of (1-x)Bi <sub>2</sub> O <sub>3</sub> -xWO <sub>3</sub> , x = 0.240, sintered at 700 °C (magnification: 1000x)	66
4.20(d)	SEM micrograph of (1-x)Bi <sub>2</sub> O <sub>3</sub> -xWO <sub>3</sub> , x = 0.250, sintered at 700 °C (magnification: 1000x)	66

4.20(e)	SEM micrograph of $(1-x)\text{Bi}_2\text{O}_3-x\text{WO}_3$ , $x = 0.255$ , sintered at $700\text{ }^\circ\text{C}$ (magnification: 1000x)	67
4.21(a)	SEM micrograph of $(1-x)\text{Bi}_2\text{O}_3-x\text{WO}_3$ , $x = 0.220$ , sintered at $900\text{ }^\circ\text{C}$ (magnification: 1000x)	67
4.21(b)	SEM micrograph of $(1-x)\text{Bi}_2\text{O}_3-x\text{WO}_3$ , $x = 0.230$ , sintered at $900\text{ }^\circ\text{C}$ (magnification: 1000x)	68
4.21(c)	SEM micrograph of $(1-x)\text{Bi}_2\text{O}_3-x\text{WO}_3$ , $x = 0.240$ , sintered at $900\text{ }^\circ\text{C}$ (magnification: 1000x)	68
4.21(d)	SEM micrograph of $(1-x)\text{Bi}_2\text{O}_3-x\text{WO}_3$ , $x = 0.250$ , sintered at $900\text{ }^\circ\text{C}$ (magnification: 1000x)	69
4.21(e)	SEM micrograph of $(1-x)\text{Bi}_2\text{O}_3-x\text{WO}_3$ , $x = 0.255$ , sintered at $900\text{ }^\circ\text{C}$ (magnification: 1000x)	69
4.22(a)	SEM micrograph of $(1-x)\text{Bi}_2\text{O}_3-x\text{WO}_3$ , $x = 0.220$ , sintered at $700\text{ }^\circ\text{C}$ , prepared via mechanochemical method (magnification: 1000x)	71
4.22(b)	SEM micrograph of $(1-x)\text{Bi}_2\text{O}_3-x\text{WO}_3$ , $x = 0.230$ , sintered at $700\text{ }^\circ\text{C}$ , prepared via mechanochemical method (magnification: 1000x)	71
4.22(c)	SEM micrograph of $(1-x)\text{Bi}_2\text{O}_3-x\text{WO}_3$ , $x = 0.240$ , sintered at $700\text{ }^\circ\text{C}$ , prepared via mechanochemical method (magnification: 1000x)	72
4.22(d)	SEM micrograph of $(1-x)\text{Bi}_2\text{O}_3-x\text{WO}_3$ , $x = 0.250$ , sintered at $700\text{ }^\circ\text{C}$ , prepared via mechanochemical method (magnification: 1000x)	72
4.22(e)	SEM micrograph of $(1-x)\text{Bi}_2\text{O}_3-x\text{WO}_3$ , $x = 0.255$ , sintered at $700\text{ }^\circ\text{C}$ , prepared via mechanochemical method (magnification: 1000x)	73
4.23(a)	SEM micrograph of $(1-x)\text{Bi}_2\text{O}_3-x\text{WO}_3$ , $x = 0.220$ , sintered at $900\text{ }^\circ\text{C}$ , prepared via mechanochemical method (magnification: 1000x)	73
4.23(b)	SEM micrograph of $(1-x)\text{Bi}_2\text{O}_3-x\text{WO}_3$ , $x = 0.230$ , sintered at $900\text{ }^\circ\text{C}$ , prepared via mechanochemical method (magnification: 1000x)	74
4.23(c)	SEM micrograph of $(1-x)\text{Bi}_2\text{O}_3-x\text{WO}_3$ , $x = 0.240$ , sintered at $900^\circ\text{C}$ , prepared via mechanochemical method (magnification: 1000x)	74
4.23(d)	SEM micrograph of $(1-x)\text{Bi}_2\text{O}_3-x\text{WO}_3$ , $x = 0.250$ , sintered at $900^\circ\text{C}$ , prepared via mechanochemical method (magnification: 1000x)	75
4.23(e)	SEM micrograph of $(1-x)\text{Bi}_2\text{O}_3-x\text{WO}_3$ , $x = 0.255$ , sintered at $900^\circ\text{C}$ , prepared via mechanochemical method (magnification: 1000x)	75
4.24(a)	SEM micrograph of $\text{Bi}_{6.24}\text{W}_{0.88}\text{O}_{12}$ , sintered at $700\text{ }^\circ\text{C}$ , prepared via mechanochemical method, milling at $700\text{ rpm}$ (magnification: 1000x)	76

4.24(b)	SEM micrograph of $\text{Bi}_{6.24}\text{W}_{0.88}\text{O}_{12}$ , sintered at 900 °C, prepared via mechanochemical method, milling at 700 rpm (magnification: 1000x)	76
4.25(a)	SEM micrograph of $\text{Bi}_{6.24}\text{W}_{0.88}\text{O}_{12}$ , sintered at 700 °C, prepared via mechanochemical method, milling at 1400 rpm (magnification: 1000x)	77
4.25(b)	SEM micrograph of $\text{Bi}_{6.24}\text{W}_{0.88}\text{O}_{12}$ , sintered at 900 °C, prepared via mechanochemical method, milling at 1400 rpm (magnification: 1000x)	77
4.26(a)	Complex impedance plane plot for $\text{Bi}_{6.24}\text{W}_{0.88}\text{O}_{12}$ synthesized via conventional solid state method (sintered at 700 °C) at 150 °C	82
4.26(b)	Complex impedance plane plot for $\text{Bi}_{6.24}\text{W}_{0.88}\text{O}_{12}$ synthesized via conventional solid state method (sintered at 700 °C) at 250 °C	82
4.26(c)	Complex impedance plane plot for $\text{Bi}_{6.24}\text{W}_{0.88}\text{O}_{12}$ synthesized via conventional solid state method (sintered at 700 °C) at 850 °C	82
4.27(a)	Complex impedance plane plot for $\text{Bi}_{6.24}\text{W}_{0.88}\text{O}_{12}$ synthesized via conventional solid state method (sintered at 900 °C) at 150 °C	83
4.27(b)	Complex impedance plane plot for $\text{Bi}_{6.24}\text{W}_{0.88}\text{O}_{12}$ synthesized via conventional solid state method (sintered at 900 °C) at 250 °C	83
4.27(c)	Complex impedance plane plot for $\text{Bi}_{6.24}\text{W}_{0.88}\text{O}_{12}$ synthesized via conventional solid state method (sintered at 900 °C) at 850 °C	83
4.28	A combined $Z''$ and $M''$ spectroscopic plots for $\text{Bi}_{6.24}\text{W}_{0.88}\text{O}_{12}$ synthesized via conventional solid state method (sintered at 700 °C) at 150 °C	85
4.29	A combined $Z''$ and $M''$ spectroscopic plots for $\text{Bi}_{6.24}\text{W}_{0.88}\text{O}_{12}$ synthesized via conventional solid state method (sintered at 900 °C) at 150 °C	86
4.30	Arrhenius plots of $\text{Bi}_{6.24}\text{W}_{0.88}\text{O}_{12}$ synthesized via conventional solid state method, sintered at two different temperatures (700 °C and 900 °C)	87
4.31	Arrhenius plots of $(1-x)\text{Bi}_2\text{O}_3-x\text{WO}_3$ , ( $0.22 \leq x \leq 0.255$ ), synthesized via conventional solid state method, sintered at 700 °C	89
4.32	Arrhenius plots of $(1-x)\text{Bi}_2\text{O}_3-x\text{WO}_3$ , ( $0.22 \leq x \leq 0.255$ ), synthesized via conventional solid state method, sintered at 900 °C	90
4.33	Arrhenius plots of $\text{Bi}_{6.24}\text{W}_{0.88}\text{O}_{12}$ synthesized via conventional solid state method, sintered at 700 °C in two different atmospheres	93
4.34	Arrhenius plots of $\text{Bi}_{6.24}\text{W}_{0.88}\text{O}_{12}$ synthesized via conventional solid	93

	state method, sintered at 900 °C in two different atmospheres	
4.35	Isothermal conductivity at 300 °C of $\text{Bi}_{6.24}\text{W}_{0.88}\text{O}_{12}$ in different atmospheres (sintered at 700 °C), synthesized via conventional solid state method	94
4.36	Isothermal conductivity at 300 °C of $\text{Bi}_{6.24}\text{W}_{0.88}\text{O}_{12}$ in different atmospheres (sintered at 900 °C), synthesized via conventional solid state method	94
4.37	Complex plot of $\text{Bi}_{6.24}\text{W}_{0.88}\text{O}_{12}$ at different applied voltages at 300 °C (sintered at 700 °C), synthesized via conventional solid state method	95
4.38	Complex plot of $\text{Bi}_{6.24}\text{W}_{0.88}\text{O}_{12}$ at different applied voltages at 300 °C (sintered at 900 °C), synthesized via conventional solid state method	95
4.39(a)	Complex impedance plane plot for $\text{Bi}_{6.24}\text{W}_{0.88}\text{O}_{12}$ prepared via mechanochemical method (sintered at 700 °C) at 150 °C	97
4.39(b)	Complex impedance plane plot for $\text{Bi}_{6.24}\text{W}_{0.88}\text{O}_{12}$ prepared via mechanochemical method (sintered at 700 °C) at 250 °C	97
4.39(c)	Complex impedance plane plot for $\text{Bi}_{6.24}\text{W}_{0.88}\text{O}_{12}$ prepared via mechanochemical method (sintered at 700 °C) at 850 °C	97
4.40(a)	Complex impedance plane plot for $\text{Bi}_{6.24}\text{W}_{0.88}\text{O}_{12}$ prepared via mechanochemical method (sintered at 900 °C) at 150 °C	98
4.40(b)	Complex impedance plane plot for $\text{Bi}_{6.24}\text{W}_{0.88}\text{O}_{12}$ prepared via mechanochemical method (sintered at 900 °C) at 250 °C	98
4.40(c)	Complex impedance plane plot for $\text{Bi}_{6.24}\text{W}_{0.88}\text{O}_{12}$ prepared via mechanochemical method (sintered at 900 °C) at 850 °C	98
4.41	A combined $Z''$ and $M''$ spectroscopic plots for $\text{Bi}_{6.24}\text{W}_{0.88}\text{O}_{12}$ prepared via mechanochemical method (sintered at 700 °C) at 150 °C	100
4.42	A combined $Z''$ and $M''$ spectroscopic plots for $\text{Bi}_{6.24}\text{W}_{0.88}\text{O}_{12}$ prepared via mechanochemical method (sintered at 900 °C) at 150 °C	101
4.43	Arrhenius plots of $\text{Bi}_{6.24}\text{W}_{0.88}\text{O}_{12}$ prepared via mechanochemical method sintered at two different temperatures (700 °C and 900 °C)	102
4.44	Arrhenius plots of $(1-x)\text{Bi}_2\text{O}_3-x\text{WO}_3$ , ( $0.220 \leq x \leq 0.255$ ), prepared via mechanochemical method, sintered at 700 °C	104
4.45	Arrhenius plots of $(1-x)\text{Bi}_2\text{O}_3-x\text{WO}_3$ , ( $0.220 \leq x \leq 0.255$ ), prepared via mechanochemical method, sintered at 900 °C	105
4.46	Arrhenius plots of $\text{Bi}_{6.24}\text{W}_{0.88}\text{O}_{12}$ prepared via mechanochemical method, sintered at 700 °C in two different atmospheres	107

4.47	Arrhenius plots of $\text{Bi}_{6.24}\text{W}_{0.88}\text{O}_{12}$ prepared via mechanochemical method, sintered at 900 °C in two different atmospheres	107
4.48	Isothermal conductivity at 300 °C of $\text{Bi}_{6.24}\text{W}_{0.88}\text{O}_{12}$ prepared via mechanochemical method, in different atmospheres (sintered at 700 °C)	108
4.49	Isothermal conductivity at 300 °C of $\text{Bi}_{6.24}\text{W}_{0.88}\text{O}_{12}$ prepared via mechanochemical method, in different atmospheres (sintered at 900 °C)	108
4.50	Complex plot of $\text{Bi}_{6.24}\text{W}_{0.88}\text{O}_{12}$ prepared via mechanochemical method, at different applied voltages at 300 °C (sintered at 700 °C)	109
4.51	Complex plot of $\text{Bi}_{6.24}\text{W}_{0.88}\text{O}_{12}$ prepared via mechanochemical method, at different applied voltages at 300 °C (sintered at 900 °C)	109
4.52	Arrhenius plots of $\text{Bi}_{6.24}\text{W}_{0.88}\text{O}_{12}$ , prepared via mechanochemical method with different milling rate (700 rpm, 1000 rpm and 1400 rpm) for 1 hour, sintered at 700 °C	111
4.53	Arrhenius plots of $\text{Bi}_{6.24}\text{W}_{0.88}\text{O}_{12}$ , prepared via mechanochemical method with different milling rate (700 rpm, 1000 rpm and 1400 rpm) for 1 hour, sintered at 900 °C	112
4.54	Arrhenius plots of $\text{Bi}_{6.24}\text{W}_{0.88}\text{O}_{12}$ prepared via two methods (conventional solid state method and mechanochemical method) and sintered at 900 °C	113
4.55	XRD patterns of Li-doped, $\text{Bi}_{6.24}\text{W}_{0.88-x}\text{Li}_x\text{O}_\delta$ ( $0 \leq x \leq 0.10$ )	116
4.56	XRD patterns of Ca-doped, $\text{Bi}_{6.24-x}\text{N}_x\text{W}_{0.88}\text{O}_\delta$ ( $0 \leq x \leq 0.95$ )	116
4.57	XRD patterns of Cu-doped, $\text{Bi}_{6.24}\text{W}_{0.88-x}\text{Cu}_x\text{O}_\delta$ ( $0 \leq x \leq 0.05$ )	116
4.58	XRD patterns of Ni-doped, $\text{Bi}_{6.24}\text{W}_{0.88-x}\text{Ni}_x\text{O}_\delta$ ( $0 \leq x \leq 0.20$ )	117
4.59	XRD patterns of Zn-doped, $\text{Bi}_{6.24}\text{W}_{0.88-x}\text{Zn}_x\text{O}_\delta$ ( $0 \leq x \leq 0.10$ )	117
4.60	XRD patterns of Cr-doped, $\text{Bi}_{6.24}\text{W}_{0.88-x}\text{Cr}_x\text{O}_\delta$ ( $0 \leq x \leq 0.15$ )	120
4.61	XRD patterns of Y-doped, $\text{Bi}_{6.24}\text{W}_{0.88-x}\text{Y}_x\text{O}_\delta$ ( $0 \leq x \leq 0.30$ )	120
4.62	XRD patterns of Sn-doped, $\text{Bi}_{6.24}\text{W}_{0.88-x}\text{Sn}_x\text{O}_\delta$ ( $0 \leq x \leq 0.20$ )	120
4.63	XRD patterns of Ti-doped, $\text{Bi}_{6.24}\text{W}_{0.88-x}\text{Ti}_x\text{O}_\delta$ ( $0 \leq x \leq 0.10$ )	121
4.64	XRD patterns of Zr-doped, $\text{Bi}_{6.24}\text{W}_{0.88-x}\text{Zr}_x\text{O}_\delta$ ( $0 \leq x \leq 0.20$ )	121
4.65	XRD patterns of Y-doped, $\text{Bi}_{6.24-x}\text{N}_x\text{W}_{0.88}\text{O}_\delta$ ( $0 \leq x \leq 0.95$ )	121

4.66	XRD patterns of Nb-doped, $\text{Bi}_{6.24}\text{W}_{0.88-x}\text{Nb}_x\text{O}_8$ ( $0 \leq x \leq 0.20$ )	124
4.67	XRD patterns of Sb-doped, $\text{Bi}_{6.24}\text{W}_{0.88-x}\text{Sb}_x\text{O}_8$ ( $0 \leq x \leq 0.15$ )	124
4.68	XRD patterns of Ta-doped, $\text{Bi}_{6.24}\text{W}_{0.88-x}\text{Ta}_x\text{O}_8$ ( $0 \leq x \leq 0.20$ )	125
4.69	XRD patterns of V-doped, $\text{Bi}_{6.24}\text{W}_{0.88-x}\text{V}_x\text{O}_8$ ( $0 \leq x \leq 0.20$ )	125
4.70	XRD patterns of Mo-doped, $\text{Bi}_{6.24}\text{W}_{0.88-x}\text{Mo}_x\text{O}_8$ ( $0 \leq x \leq 0.50$ )	125
4.71	TGA thermograms of Li, Cu, Ni and Zn substituted W in $\text{Bi}_{6.24}\text{W}_{0.88}\text{O}_{12}$ from room temperature to 910 °C: (a) $\text{Bi}_{6.24}\text{W}_{0.78}\text{Li}_{0.10}\text{O}_{11.750}$ ; (b) $\text{Bi}_{6.24}\text{W}_{0.83}\text{Cu}_{0.05}\text{O}_{11.900}$ ; (c) $\text{Bi}_{6.24}\text{W}_{0.68}\text{Ni}_{0.20}\text{O}_{11.600}$ ; (d) $\text{Bi}_{6.24}\text{W}_{0.78}\text{Zn}_{0.10}\text{O}_{11.800}$	129
4.72	TGA thermograms of Cr, Y, Ti and Sn substituted W in $\text{Bi}_{6.24}\text{W}_{0.88}\text{O}_{12}$ from room temperature to 910°C: (a) $\text{Bi}_{6.24}\text{W}_{0.73}\text{Cr}_{0.15}\text{O}_{11.775}$ ; (b) $\text{Bi}_{6.24}\text{W}_{0.68}\text{Y}_{0.30}\text{O}_{11.550}$ (c) $\text{Bi}_{6.24}\text{W}_{0.78}\text{Ti}_{0.10}\text{O}_{11.900}$ ; (d) $\text{Bi}_{6.24}\text{W}_{0.68}\text{Sn}_{0.20}\text{O}_{11.800}$	130
4.73	TGA thermograms of Zr, Ta, V and Nb substituted W in $\text{Bi}_{6.24}\text{W}_{0.88}\text{O}_{12}$ from room temperature to 910°C: (a) $\text{Bi}_{6.24}\text{W}_{0.68}\text{Zr}_{0.20}\text{O}_{11.800}$ ; (b) $\text{Bi}_{6.24}\text{W}_{0.68}\text{Ta}_{0.20}\text{O}_{11.900}$ (c) $\text{Bi}_{6.24}\text{W}_{0.68}\text{V}_{0.20}\text{O}_{11.900}$ ; (d) $\text{Bi}_{6.24}\text{W}_{0.68}\text{Nb}_{0.20}\text{O}_{11.900}$	130
4.74	TGA thermograms of Sb and Mo substituted W and Ca and Y-doped substituted Bi in $\text{Bi}_{6.24}\text{W}_{0.88}\text{O}_{12}$ from room temperature to 910°C: (a) $\text{Bi}_{6.24}\text{W}_{0.73}\text{Sb}_{0.15}\text{O}_{11.925}$ ; (b) $\text{Bi}_{6.24}\text{W}_{0.38}\text{Mo}_{0.50}\text{O}_{11.900}$ (c) $\text{Bi}_{5.29}\text{Ca}_{0.95}\text{W}_{0.88}\text{O}_{11.525}$ ; (d) $\text{Bi}_{5.29}\text{Y}_{0.95}\text{W}_{0.88}\text{O}_{11.525}$	131
4.75	IR spectra of $\text{Bi}_{6.24}\text{W}_{0.88-x}\text{Li}_x\text{O}_8$ solid solutions: (a) $x=0.02$ ; (b) $x=0.05$ ; (c) $x=0.10$	132
4.76	IR spectra of $\text{Bi}_{6.24}\text{W}_{0.88-x}\text{Cu}_x\text{O}_8$ solid solutions: (a) $x=0.02$ ; (b) $x=0.05$	133
4.77	IR spectra of $\text{Bi}_{6.24}\text{W}_{0.88-x}\text{Ni}_x\text{O}_8$ solid solutions: (a) $x=0.05$ ; (b) $x=0.10$ ; (c) $x=0.15$ ; (d) $x=0.20$	133
4.78	IR spectra of $\text{Bi}_{6.24}\text{W}_{0.88-x}\text{Zn}_x\text{O}_8$ solid solutions: (a) $x=0.02$ ; (b) $x=0.05$ ; (c) $x=0.10$	133
4.79	IR spectra of $\text{Bi}_{6.24-x}\text{Ca}_x\text{W}_{0.88}\text{O}_8$ solid solutions: (a) $x=0.10$ ; (b) $x=0.30$ ; (c) $x=0.60$ ; (d) $x=0.95$	134
4.80	IR spectra of $\text{Bi}_{6.24}\text{W}_{0.88-x}\text{Cr}_x\text{O}_8$ solid solutions: (a) $x=0.05$ ; (b) $x=0.10$ ; (c) $x=0.15$	134
4.81	IR spectra of $\text{Bi}_{6.24}\text{W}_{0.88-x}\text{Y}_x\text{O}_8$ solid solutions: (a) $x=0.05$ ; (b) $x=0.10$ ; (c) $x=0.20$ ; (d) $x=0.30$	134

4.82	IR spectra of $\text{Bi}_{6.24-x}\text{Y}_x\text{W}_{0.88}\text{O}_\delta$ solid solutions: (a) $x=0.10$ ; (b) $x=0.30$ ; (c) $x=0.60$ ; (d) $x=0.95$	135
4.83	IR spectra of $\text{Bi}_{6.24}\text{W}_{0.88-x}\text{Sn}_x\text{O}_\delta$ solid solutions: (a) $x=0.05$ ; (b) $x=0.10$ ; (c) $x=0.15$ ; (d) $x=0.20$	135
4.84	IR spectra of $\text{Bi}_{6.24}\text{W}_{0.88-x}\text{Ti}_x\text{O}_\delta$ solid solutions: (a) $x=0.02$ ; (b) $x=0.05$ ; (c) $x=0.10$	135
4.85	IR spectra of $\text{Bi}_{6.24}\text{W}_{0.88-x}\text{Zr}_x\text{O}_\delta$ solid solutions: (a) $x=0.05$ ; (b) $x=0.10$ ; (c) $x=0.15$ ; (d) $x=0.20$	136
4.86	IR spectra of $\text{Bi}_{6.24}\text{W}_{0.88-x}\text{Nb}_x\text{O}_\delta$ solid solutions: (a) $x=0.05$ ; (b) $x=0.10$ ; (c) $x=0.15$ ; (d) $x=0.20$	136
4.87	IR spectra of $\text{Bi}_{6.24}\text{W}_{0.88-x}\text{Sb}_x\text{O}_\delta$ solid solutions: (a) $x=0.05$ ; (b) $x=0.10$ ; (c) $x=0.15$	136
4.88	IR spectra of $\text{Bi}_{6.24}\text{W}_{0.88-x}\text{Ta}_x\text{O}_\delta$ solid solutions: (a) $x=0.05$ ; (b) $x=0.10$ ; (c) $x=0.15$ ; (d) $x=0.20$	137
4.89	IR spectra of $\text{Bi}_{6.24}\text{W}_{0.88-x}\text{V}_x\text{O}_\delta$ solid solutions: (a) $x=0.05$ ; (b) $x=0.10$ ; (c) $x=0.15$ ; (d) $x=0.20$	137
4.90	IR spectra of $\text{Bi}_{6.24}\text{W}_{0.88-x}\text{Mo}_x\text{O}_\delta$ solid solutions: (a) $x=0.05$ ; (b) $x=0.10$ ; (c) $x=0.20$ ; (d) $x=0.30$ ; (e) $x=0.40$ ; (f) $x=0.50$	137
4.91	SEM micrograph of $\text{Bi}_{6.24}\text{W}_{0.78}\text{Li}_{0.10}\text{O}_{11.750}$ (magnification: 1000x)	142
4.92	SEM micrograph of $\text{Bi}_{6.24}\text{W}_{0.83}\text{Cu}_{0.05}\text{O}_{11.900}$ (magnification: 1000x)	142
4.93	SEM micrograph of $\text{Bi}_{6.24}\text{W}_{0.68}\text{Ni}_{0.20}\text{O}_{11.600}$ (magnification: 1000x)	143
4.94	SEM micrograph of $\text{Bi}_{6.24}\text{W}_{0.78}\text{Zn}_{0.10}\text{O}_{11.800}$ (magnification: 1000x)	143
4.95	SEM micrograph of $\text{Bi}_{6.24}\text{W}_{0.73}\text{Cr}_{0.15}\text{O}_{11.775}$ (magnification: 1000x)	144
4.96	SEM micrograph of $\text{Bi}_{6.24}\text{W}_{0.78}\text{Ti}_{0.10}\text{O}_{11.900}$ (magnification: 1000x)	144
4.97	SEM micrograph of $\text{Bi}_{6.24}\text{W}_{0.78}\text{Sn}_{0.10}\text{O}_{11.900}$ (magnification: 1000x)	145
4.98	SEM micrograph of $\text{Bi}_{6.24}\text{W}_{0.68}\text{Zr}_{0.20}\text{O}_{11.800}$ (magnification: 1000x)	145
4.99	SEM micrograph of $\text{Bi}_{6.24}\text{W}_{0.68}\text{Ta}_{0.20}\text{O}_{11.900}$ (magnification: 1000x)	146
4.100	SEM micrograph of $\text{Bi}_{6.24}\text{W}_{0.68}\text{Nb}_{0.20}\text{O}_{11.900}$ (magnification: 1000x)	146
4.101	SEM micrograph of $\text{Bi}_{6.24}\text{W}_{0.73}\text{Sb}_{0.15}\text{O}_{11.925}$ (magnification: 1000x)	147
4.102	SEM micrograph of $\text{Bi}_{6.24}\text{W}_{0.38}\text{Mo}_{0.50}\text{O}_{12.000}$ (magnification: 1000x)	147

4.103	SEM micrograph of $\text{Bi}_{5.29}\text{Ca}_{0.95}\text{W}_{0.88}\text{O}_{11.525}$ (magnification: 1000x)	148
4.104	SEM micrograph of $\text{Bi}_{5.29}\text{Y}_{0.95}\text{W}_{0.88}\text{O}_{11}$ (magnification: 1000x)	148
4.105	Arrhenius plots of Li-doped, $\text{Bi}_{6.24}\text{W}_{0.88-x}\text{Li}_x\text{O}_\delta$ ( $0 \leq x \leq 0.10$ )	150
4.106	Arrhenius plots of Ca-doped, $\text{Bi}_{6.24-x}\text{N}_x\text{W}_{0.88}\text{O}_\delta$ ( $0 \leq x \leq 0.95$ )	151
4.107	Arrhenius plots of Cu-doped, $\text{Bi}_{6.24}\text{W}_{0.88-x}\text{Cu}_x\text{O}_\delta$ ( $0 \leq x \leq 0.05$ )	152
4.108	Arrhenius plots of Ni-doped, $\text{Bi}_{6.24}\text{W}_{0.88-x}\text{Ni}_x\text{O}_\delta$ ( $0 \leq x \leq 0.20$ )	153
4.109	Arrhenius plots of Zn-doped, $\text{Bi}_{6.24}\text{W}_{0.88-x}\text{Zn}_x\text{O}_\delta$ ( $0 \leq x \leq 0.10$ )	154
4.110	Arrhenius plots of Cr-doped, $\text{Bi}_{6.24}\text{W}_{0.88-x}\text{Cr}_x\text{O}_\delta$ ( $0 \leq x \leq 0.15$ )	157
4.111	Arrhenius plots of Y-doped, $\text{Bi}_{6.24}\text{W}_{0.88-x}\text{Y}_x\text{O}_\delta$ ( $0 \leq x \leq 0.30$ )	158
4.112	Arrhenius plots of Y-doped, $\text{Bi}_{6.24-x}\text{N}_x\text{W}_{0.88}\text{O}_\delta$ ( $0 \leq x \leq 0.95$ )	159
4.113	Arrhenius plots of Sn-doped, $\text{Bi}_{6.24}\text{W}_{0.88-x}\text{Sn}_x\text{O}_\delta$ ( $0 \leq x \leq 0.10$ )	160
4.114	Arrhenius plots of Ti-doped, $\text{Bi}_{6.24}\text{W}_{0.88-x}\text{Ti}_x\text{O}_\delta$ ( $0 \leq x \leq 0.10$ )	161
4.115	Arrhenius plots of Zr-doped, $\text{Bi}_{6.24}\text{W}_{0.88-x}\text{Zr}_x\text{O}_\delta$ ( $0 \leq x \leq 0.20$ )	162
4.116	Arrhenius plots of Nb-doped, $\text{Bi}_{6.24}\text{W}_{0.88-x}\text{Nb}_x\text{O}_\delta$ ( $0 \leq x \leq 0.20$ )	164
4.117	Arrhenius plots of Sb-doped, $\text{Bi}_{6.24}\text{W}_{0.88-x}\text{Sb}_x\text{O}_\delta$ ( $0 \leq x \leq 0.15$ )	165
4.118	Arrhenius plots of Ta-doped, $\text{Bi}_{6.24}\text{W}_{0.88-x}\text{Ta}_x\text{O}_\delta$ ( $0 \leq x \leq 0.20$ )	166
4.119	Arrhenius plots of V-doped, $\text{Bi}_{6.24}\text{W}_{0.88-x}\text{V}_x\text{O}_\delta$ ( $0 \leq x \leq 0.20$ )	167
4.120	Arrhenius plots of Mo-doped, $\text{Bi}_{6.24}\text{W}_{0.88-x}\text{Mo}_x\text{O}_\delta$ ( $0 \leq x \leq 0.50$ )	168

## LIST OF ABBREVIATIONS

AC	alternating current
dc	direct current
FT-IR	Fourier-transform infrared spectroscopy
ICSD	international centre for diffraction data
SEM	scanning electron microscopy
TGA	thermogravimetry analysis
XRD	X-ray Diffraction
C	capacitance
$C_b$	bulk capacitance
$C_o$	vacuum capacitance
$C_{dl}$	double layer capacitance
$C_{gb}$	grain boundary capacitance
d	d-spacing
$E_a$	activation energy
eV	electron volt
f	frequency
h, k, l	milller indices
I	current
k	Boltzmann's constant
K	kelvin
$l$	thickness
$M^*$	complex electric modulus
$M'$	real part of electric modulus
$M''$	imaginary part of electric modulus

$R$	resistance
$R_b$	bulk resistance
$R_{gb}$	grain boundary resistance
$RC$	resistor-capacitor
$T$	temperature
$V$	voltage
$Z$	impedance
$Z^*$	complex impedance
$Z'$	real part of impedance
$Z''$	imaginary part of impedance
$\Omega$	ohm
$\rho$	resistivity
$\epsilon^*$	complex permittivity
$\epsilon_r$	relative permittivity
$\tan \delta$	dielectric loss
$\omega$	angular frequency
$\lambda$	wavelength

## CHAPTER 1

### INTRODUCTION

#### 1.1 Electroceramics

Ceramic materials can be divided into traditional ceramics and advanced ceramics. In the early civilizations, traditional ceramics are pottery, structural clay products, clay-based refractories, cements, concretes and glasses. Recent year, attention is focused on advanced ceramics, which refer to the ceramics for electrical, magnetic, electronic and optical applications (functional ceramics) and structural ceramics at ambient and elevated temperatures. Traditionally, high electrical resistance ceramic materials are utilized for electrical insulation. In modern days, oxides and oxide compounds employed in the ceramic technology possess high electrical conductivity, either ionic or electronic (Moulson and Herbert, 2003; Rahaman, 2003).

The foundations of electroceramics are the science of ceramic processing, chemistry and solid state physics with its products find applications in diverse fields. Electroceramics is a trans-disciplinary, both in fundamentals and applications aspects. Dielectric ceramics are referred to those linear and non-linear dielectrics. In contrast, conductive ceramics consists of super-conductors, conductors and semiconductors (including ionically and electronically conductive ceramics). In addition, magnetic ceramics and optical ceramics are electroceramics material too (Setter, 2001).

Electroceramics are high technology materials whose properties and applications depend on the close control of structure, composition, ceramic texture, type of dopants and dopant (or defect) distribution. Some ceramics, like 'fast-ion conductors', which could conduct electricity well and predominantly by the transport of ions, thus they contribute crucial roles in fuel cell and sensor technologies. They are present as integral components of the circuit used in computers, signal processing, telecommunications, power transmission and power control technologies due to their wide range of properties such as polarisation, mechanical and optical responses, which may be controlled through composition, chemical substitution, doping and fabrication conditions. There are a few examples of the development in electroceramics technology, include ferroelectric research and development, alumina developments for thick-film microelectronics in oxide ceramics and high thermal conductivity ceramics for integrated circuit packaging (Steele, 1991; Levinson, 1987). Table 1.1 lists out some examples of electroceramics.

**Table 1.1: Examples of electroceramics**

<b>Materials</b>	<b>Properties</b>	<b>Applications</b>
BaTiO-based	High dielectric permittivity	Small plate capacitors, tube capacitors and multilayer capacitors (MLCs)
Pb(Ti, Zr)O <sub>3</sub>	Piezoelectric	Sensors, actuators, ultrasonic transducer and electro-acoustic
n-doped semiconducting BaTiO <sub>3</sub>	grain boundaries barrier controlled, positive temperature coefficient (PTC) of the resistivity	self-controlled electrical heating systems
ZrO <sub>2</sub>	Ionic conductor	Electrochemical oxygen sensors in cars and high-temperature solid oxide fuel cells (SOFCs)
ZnO	strongly non-linear current-voltage behavior	Overvoltage protection varistors
YBa <sub>2</sub> CuO <sub>7</sub>	high-temperature superconducting ceramics	power applications as high-voltage energy transmission cables and magnetic energy storage

## 1.2 Solid Oxide Electrolyte

### 1.2.1 Overview

Electrical conduction occurs by the long range diffusion of either electrons or ions. Predominant one charge carrier (electron or ion) causes the conduction to occur in a material. Meanwhile, in certain organic materials, mix charge carrier conduction of ionic and electronic is significant.

Solid electrolytes, fast ion conductors and superionic conductors refer to one set of ions that can move easily. They show high conductivity in the absence of a significant electronic contribution. Such materials often have rather special crystal structures with open tunnels or layers through which the mobile ions may move. The conductivity values, example  $10^{-3} \text{ ohm}^{-1} \text{ cm}^{-1}$  for Na<sup>+</sup> ion migration in  $\beta$ -alumina at (25 °C) is comparable to those observed for strong liquid electrolytes. It is now apparent from both theoretical and experimental results on a wide variety of materials that ionic conductivities of  $0.1 \text{ ohm}^{-1} \text{ cm}^{-1}$  to  $10.0 \text{ ohm}^{-1} \text{ cm}^{-1}$  are the maximum that are likely to be obtained for any material. These values are obtained when a large proportion of the ions move at any one time.

Most crystalline materials have low ionic conductivities because the atoms or ion

vibrate at their lattice sites and cannot move freely, escape from their lattice sites. For example, NaCl is an insulator at room temperature (conductivity around  $10^{-15}$  ohm<sup>-1</sup> cm<sup>-1</sup>). This phenomenon does not observe for solid electrolytes materials, where cations or anions are free to move throughout the whole structure. Consequently, they are intermediate between normal crystalline solids and liquid electrolytes. Figure 1.1 depicts solid electrolytes as intermediate between normal crystalline solids and liquids. Figure 1.2 shows the electrical conductivities of several common substances.

Solid electrolytes have conductivities that fall between those of a typical semiconductor, silicon and a typical aqueous electrolyte, sodium chloride. They are stable only at high temperatures. Otherwise, they may undergo a phase transition to a polymorph with a low ionic conductivity on cooling. For example, AgI is poor conductor at 25 °C. However, its structure changes to polymorph,  $\alpha$ -AgI (phase transition), which has mobile Ag<sup>+</sup> ions on heating, lead to conductivity increases.

There has been many potential applications of solid electrolytes, include fuel cells, sensors, electrochromic materials for both optical display and 'smart window' devices, low-cost electrolysis of water and selective atomic filters. Oxygen detectors for automotive pollution-control systems employ solid O<sup>2-</sup> conductors and solid-state batteries using Li<sup>+</sup> conducting solid electrolytes are the devices of solid electrolytes.

### 1.2.2 Conduction Mechanism

In ionic crystal, the individual lattice atoms transfer electrons between each other to form positively charged cations (donate electrons) and negatively charged anions (accept electrons). This strong natural binding force between cations and anions is known as electrostatic. The conductivity of ionic crystals is about twenty two orders of magnitude smaller than the conductivity of typical metallic conductors at room temperature. This could be attributed to the wide band-gap in insulators that allows few electrons to excite from the valance into the conduction bands (Hummel, 1992).

During ionic conduction, ions are charge carriers because the cations or anions are free to move throughout the structure. There are two requirements must be fulfilling either in order for ions to move freely: (i) some lattice sites must be vacant to allow the adjacent ions to hop into the vacancies and leaving their own sites vacant, or (ii) available interstitial sites for ions in interstitial sites hop into the adjacent interstitial sites.

Besides, sufficient energy to pass over an energy barrier is required in order for ions to move through a crystalline solid. Thus, ionic conduction is easier at higher temperatures as ions vibrate more vigorously and defect concentrations are higher. A highly polarized anion framework is needed for significant ionic conduction. Some factors that must be satisfied in order to obtain high ionic conductivity of ceramics are high density of mobile ions, the availability of vacant sites that can be accessed by the

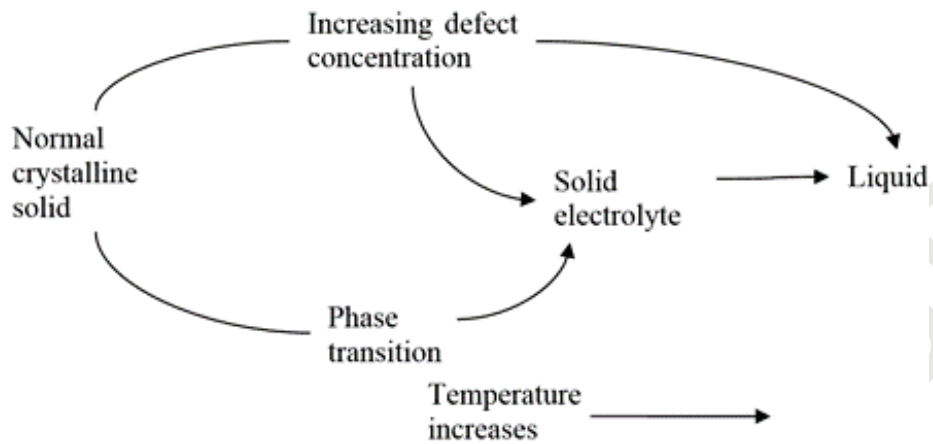


Figure 1.1: Solid electrolytes as intermediate between normal crystalline solids and liquids (West, 1999)

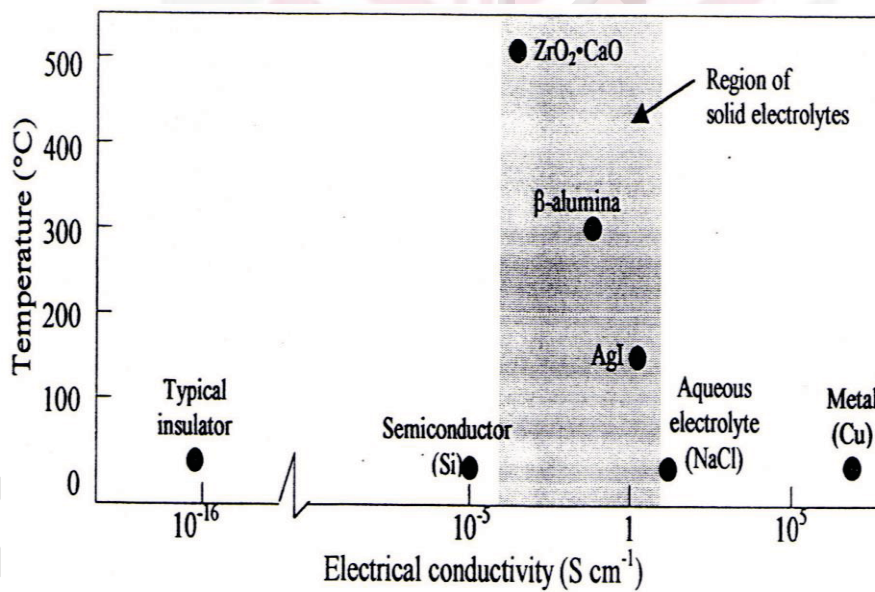


Figure 1.2: Electrical conductivities of selected common substances and representative solid electrolytes (Greenblatt, 1994)

mobile ions and good connectivity among the sites (requiring conduction channels with low free energy ( $E_a$ ) barriers between the sites).

For any material and charge carrier, the specific conductivity,  $\sigma$ , is given by

$$\sigma = \sum_i n_i e_i \mu_i \quad (1.1)$$

For ionic conductivity,  $\sigma$ ,

$$\sigma = N_{\text{ion}} e \mu_{\text{ion}} \quad (1.2)$$

where  $N_{\text{ion}}$  is the number of ions which can change their positions under the influence of an electric field,  $e$  is elementary charge and  $\mu_{\text{ion}}$  is the mobility of ions.

Arrhenius law shows the correlation between the conductivity and temperature (Corumle et al., 2015). It can be represented by the formula:

$$\sigma = \sigma_0 \exp(-E_a/kT) \quad (1.3)$$

where  $\sigma$  is oxygen ion conductivity,  $\sigma_0$  is the pre-exponential factor,  $E_a$  is the apparent activation energy for oxygen migration,  $k$  is the Boltzmann constant and  $T$  is the absolute temperature (K).

Oxide ion conductors are ionic conductors as advanced ceramic materials in which oxide ions (anions) act as charge carriers. They are very useful for a number of electrochemical devices, including solid oxide fuel cells (SOFCs) and oxygen sensors.

### 1.2.3 Application

#### 1.2.3.1 Solid Oxide Fuel Cells (SOFC)

Fuel cells are electrochemical energy conversion devices that generate electricity and heat by converting the chemical energy of fuels without combustion as an intermediate step. It converts gaseous fuels (hydrogen, natural gas and gasified coal) via an electrochemical process directly into electricity. This direct use of hydrocarbon fuels greatly decreases the complexity and cost of the fuel cell system. It does not produce significant amounts of pollutants compared with internal combustion engines. It is environmentally friendly operation, low noise, high efficient and compact in the generation of electricity through chemistry instead of combustion.

Fuel cells and batteries can be connected together in series to produce higher voltages. However, a battery is an energy storage device that stores its fuel internally and that can only supply a fixed amount of energy. In contrast, fuel cell does not need to be recharged and generates electricity as long as fuel and water are supplied externally. Fuel cell has no fixed capacity and can accept almost all kind of fuel, including natural gas, coal gas, gaseous fuels from biomass and liquid fuels (Badwal and Foger, 1995).

Generally, there are four types of fuel cells – solid oxide, proton exchange membrane, molten carbonate and alkaline. Solid oxide fuel cells (SOFCs) are the most attractive because they have the highest efficiencies and the potential of using many fuels, including gasoline and diesel, without expensive external reformers that create more volatile chemicals compare to any conventional fuel cell design. It is significant to environmental benefits. It can operate at high temperatures, producing high-grade exhaust, which can be recovered and used for other applications, such as space heating and cooling, and generating extra electricity by spinning a gas turbine linked to the unit.

As a power generator, it can convert more than 55 % of the energy in its fuel source to electricity. Its efficiency is much higher than that of conventional coal plants (efficiencies around 34 %). When the high-quality exhaust from the electrochemical process is used, overall efficiencies of a SOFC could reach 85 % (Badwal and Foger, 1995).

Besides, solid oxide fuel cells have a wide variety of applications from use as auxiliary power units in vehicles to stationary power generation with outputs from 100 W to 2 MW. A compact SOFC system can supply a maximum power of 64 kW for driving and that the system efficiency is 3 to 4 times higher than an internal combustion engine system. During the past few years, developments in ceramics for solid oxide fuel cells in lowering of the operating temperature from 1000°C to 800°C with improved conductivity characteristics, has been achieved by reducing the thickness and polarisation losses over the cell interfaces, allowing better electrochemical performance (Arespacochaga *et al.*, 2015; Mahato *et al.*, 2015).

SOFCs are made from solid state materials, namely ceramic oxides. Figure 1.3 reveals SOFC consists of three components: a cathode, an anode and an electrolyte (sandwiched between cathode and anode). A dense electrolyte is favourable as a good ion conducting characteristics and low electronic conductivity. Charge carriers in the electrolyte are oxygen species. The electrolyte is a nonporous ceramic material with ion conducting oxide.

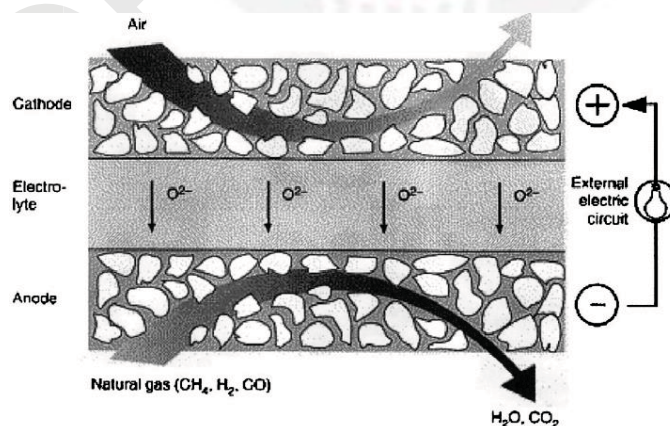


**Figure 1.3: Schematic of a ceramic fuel cell or solid oxide fuel cell (SOFC) (Huijsmans, 2001)**

At cathode, oxygen (from air) accepts electrons from external circuit and is reduced to negatively charged oxygen ions ( $O^{2-}$ ). These ions travel through the solid electrolyte to the anode, where they react with fuel at the anode. The fuel is oxidized by the oxygen ions and releases electrons to an external circuit, thereby producing electricity. In other words, electrochemical reduction of oxygen occurs at the cathode and the oxygen passes through the electrolyte membrane via a vacancy mechanism to the anode. At the anode, electrochemical oxidation of hydrogen occurs, where the hydrogen is provided from directly reformed natural gas or other hydrocarbons. The solid electrolyte conducts these ions between the electrodes, thus maintaining overall electrical charge balance and the flow of electrons in the external circuit provides useful power.

Fuel cell stack is the connection of several single cells in series using electrical interconnections to achieve higher voltages. Traditionally, the SOFC electrolyte is yttrium-stabilised zirconia (YSZ) at the extremely high operation temperature (around 1000 °C) over the years because of its oxide ion concentration and its chemical stability in reducing and oxidising atmospheres. This high operating temperature is a major problem which accelerates the degradation of cell components as well as limit choices of cell components. Therefore, the increment cost in fabrication of cell components is unavoidable.

New electrolytes with higher oxygen conductivity and negligible electrical conductivity that could be applied in the SOFC with lower operation temperature compare to YSZ are required in order to reduce materials costs and improve chemical and mechanical stability of the ceramics (Shao *et al.*, 2012; Pelosato *et al.*, 2015).

### 1.2.3.2 Oxygen Sensor

In solid electrolytes, the conductivity of a solid electrolyte due to the mobility of oxygen ion,  $O^{2-}$ , is very low at room temperature and comparable to that of an aqueous electrolyte when temperatures achieve above 600 °C. If the operation temperature is not too high or the oxygen partial pressure is not too low, the conductivity due to the electron mobility can be neglected and pure oxygen ion conduction is assumed. This property is utilized in oxygen concentration cells containing solid electrolytes for the measurement of oxygen partial pressures in gas mixtures or concentrations of gases in liquids.

Oxygen sensors apply in automobiles to control the combustion for the internal combustion engine (air/fuel ratio). However, The main concern of such sensors as oxygen concentration cell are thermal resistance requirement under the exposure to the high temperature exhaust gas up to 1000 °C, gas tightness against the exhaust gas pressure and intensity warranty to endure mechanical shocks. Yttrium stabilize zirconia is currently selected as sensor due to the electrical conduction, mechanical toughness and easily obtainable.

Figure 1.4 depicts the operation principle for oxygen sensor. An oxygen concentration

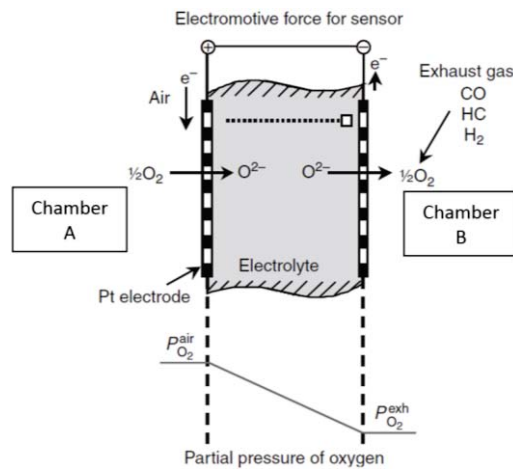


**Figure 1.4: The operation principle for oxygen sensor (Yamada, T. 2003)**

cell can be constructed by separating two gas chambers (chamber A and B) by an oxygen ion conducting solid electrolyte. Along the border of the solid electrolyte wall, oxide ion is transferred in a direction that reduces the difference of oxygen partial pressure between chamber A and chamber B. Electromotive force is generated and measured. This is known as an oxygen concentration cell. The output will be related to the logarithm of the ratio of the partial pressures of oxygen at each of the electrodes as given by the Nernst equation:

$$\text{Electromotive force} = (RT/4F) \ln (P_a/P_b) \quad (1.4)$$

where R is the gas constant, T is absolute temperature, F is Faraday constant, P<sub>a</sub> is oxygen partial pressure in the high oxygen concentration chamber A (oxygen partial pressure in the ambient air/reference material) and P<sub>b</sub> is oxygen partial pressure in the low oxygen concentration chamber B (oxygen partial pressure in the exhaust gas/sample). Consequently, when a non-combusting mixture of known oxygen concentration is used as reference (air), the partial pressure of oxygen in the gas mixture of the sample may be determined.

### 1.3 Solid Solutions

A solid solution is a crystalline phase that can have variable compositions. Simple solid solutions are divided into two types in doped crystals, which are substitutional solid solutions and interstitial solid solutions.

In substitutional solid solutions, the atom or ion that is being introduced directly replaces an atom or ion of the same charge (homovalent) in the parent structure. There are a few requirements to be fulfilled for a range of simple substitutional solid solutions to form. First, the atom or ion must be the same charge as mentioned above. Second, the ions that replace each other must be fairly similar in size. A difference of 15 per

cent in the radii of the metal atoms that replace each other is the most that can be tolerated for the formation of a substantial range of solid solutions.

In non-metallic systems solid solutions, the limit is above than 15 per cent, but it is difficult to quantify this in term of the sizes of the ions and the formation of the solid solutions is very temperature dependent. Consequently, formation of extensive solid solutions often needs high temperatures, whereby the formation of solid solutions at lower temperatures may be more restricted or hardly exist. Ions with similar size may substitute for each other easily and extensive solid solutions that are stable at all temperatures may be formed. For ions that differ in size by 15 to 20 per cent, solid solutions will be formed at high temperatures and with the ionic size differs by more than around 30 per cent, solid solutions are not expected to form. The crystal structure of the two end members of a solid solution is an important factor to consider in the formation of solid solutions. If a complete solid solution series is formed, the end members must be isostructural but conversely, if two phases are isostructural, it is not necessary that a complete solid solution series is formed. Generally, it is common to have partial or limited ranges of solid solutions (West, 1999)

For the formation of interstitial solid solutions, the introduced species occupies a site that is normally empty and no ions or atoms are left out in the formation of interstitial solid solutions. This type of substitution is generally observed in metals in which small atoms such as H, C and N enter empty interstitial sites within the host metal structure.

Besides the simple solid solutions discussed above, there are more complex solid solution formation mechanisms which involved heterovalent or aliovalent substitution (ions are substituted by other ions of different charges). Thus, additional changes involving creation of vacancies or interstitials (ionic compensation) or electrons or holes (electronic compensation) are needed.

For ionic compensation, substitution host cations with higher valence species results in creation of cation vacancies or interstitial anions. Meanwhile, anion vacancies or interstitial cations are created when lower valence species substitute for host cations in a crystal. Thus, cation or anion vacancies can be created to preserve electro-neutrality. Alternatively, interstitial can be created. However, this mechanism is not common because most structures do not have interstitial sites large enough to accommodate extra cations or anions (West, 1999).

There is also another type of substitution called double substitution in which two substitutions take place simultaneously to give solid solutions. The substituting ions may be of difference charge, as long as the overall electro-neutrality is preserved. The mechanism for formation of solid solutions in many metal containing materials and especially in those that have mixed valency involves electronic compensation. This yields products which are semiconducting or metallic, or superconducting at low temperatures. Some examples of this mechanism are generation of cation vacancies by deintercalation, creation of mixed valency cations with insertion of interstitial anions into the structure and creation of interstitial cations of one element and mixed valency

cations of another element which arises from intercalation. This type of phenomena is seen in electrode materials such as  $\text{LiMn}_2\text{O}_4$ ,  $\text{LiCo}_2\text{O}_4$ ,  $\text{LiWO}_3$  and superconductor such as  $\text{YBa}_2\text{Cu}_3\text{O}_8$  (West, 1999).

#### 1.4 Problem Statements

Fabrication of fuel cells is costly. This is because the currently used electrolyte, yttria-stabilized zirconia (YSZ), only could demonstrates high ionic conductivity at high operating temperature (around 1000 °C) in fuel cell. Durability is another limitation as fuel cell might suffer after the cell repeatedly heats up to high operating temperature and then cools down to room temperature. Moreover, solid oxide systems may have issues with material corrosion, materials aging, undesirable chemical reaction between cell components (like electrolyte, electrodes, and interconnecting material) and precious of the cell components (like platinum) is needed in order to withstand such high operating temperature. In short, precise detailed knowledge of fuel cell electrochemical operations is the main goal that should be obtained in purpose to solve these fuel cell challenges (Mahato *et al.*, 2015).

$\delta\text{-Bi}_2\text{O}_3$  exhibits higher ionic conductivity than zirconia based electrolytes. However, it has low melting point (824 °C) and can only exist in a narrow stability range (between 730 °C to 825 °C) (Niu *et al.*, 2011).  $\text{Bi}^{3+}$  in the compounds can be reduced to metallic Bi state in a reducing atmosphere at high temperature (oxygen pressure less than  $10^{-7}$  Pa at 670 °C) (Katayama *et al.*, 2011). Therefore, this unstable of thermodynamic phase change of  $\text{Bi}_2\text{O}_3$ -based materials is a disadvantages for the application as SOFC electrolyte (Lin and Wei, 2011).

Bismuth based tungsten oxide materials with a general formula of  $(1-x)\text{Bi}_2\text{O}_3\text{-}x\text{WO}_3$ , ( $0.220 \leq x \leq 0.255$ ), were studied.  $\text{WO}_3$  was chosen as dopant in this present work to introduce into  $\text{Bi}_2\text{O}_3$ . The introduction of more oxygen atoms by doping with high charge valence,  $\text{W}^{6+}$ , is believed could suppress the phase transition which cause by the present of oxygen vacancies in  $\text{Bi}_2\text{O}_3$  structure. Two synthesis methods, conventional solid state and mechanochemical method, were selected to evaluate their suitability in synthesizing the desired single phase material at the best synthesis condition (lower temperature and shorter duration). The outcome is believed could provide a useful guideline, specifically for large scale of ceramic production in industrial.

There are few targets of the present work. A material that can present a higher stability at different temperatures with varying oxygen partial pressure and changes of atmospheres is desired as a solid electrolyte in SOFC. In other words, this material does not undergo decomposition to other phase or degradation of ionic conductivity under any conditions in a wide range of temperature (room temperature to 1000 °C). In addition, it will be excellent if a pure oxide ion electrolyte is produced which demonstrates higher ionic conductivity than the current electrolyte (YSZ) at comparable temperature. Therefore, this can accelerate the performance of a fuel cell.

Recent progress in chemical doping is another option to modify the behaviour of a material, specifically the electrical property. Generally, amount of oxide ion vacancy is correlated well with variations in conductivity of doped materials. It is worthy to mention that such phenomenon may or may not be the only one significant criteria in determining the electrical behaviour of a material. Ionic potential cation and unit cell parameters are two other factors that do play a role in determining the variation of electrical conductivity in a material.

### 1.5 Objectives

The objectives of this study are:

1. To prepare  $(1-x)\text{Bi}_2\text{O}_3-x\text{WO}_3$ , ( $0.220 \leq x \leq 0.255$ ), via conventional solid state and mechanochemical methods.
2. To characterize the single phase materials using X-ray powder diffraction (XRD), thermogravimetry analysis (TGA), scanning electron microscopy (SEM), Fourier-transform infrared spectroscopy (FT-IR) and X-ray fluorescence (XRF) spectroscopy.
3. To study the electrical properties of single phase materials using AC impedance spectroscopy.
4. To prepare and characterize chemically doped materials in  $\text{Bi}_{6.24}\text{W}_{0.88}\text{O}_{12}$  by using monovalent ( $\text{Li}^+$ ), divalent ( $\text{Ca}^{2+}$ ,  $\text{Cu}^{2+}$ ,  $\text{Ni}^{2+}$  and  $\text{Zn}^{2+}$ ), trivalent ( $\text{Cr}^{3+}$  and  $\text{Y}^{3+}$ ), tetravalent ( $\text{Sn}^{4+}$ ,  $\text{Ti}^{4+}$  and  $\text{Zr}^{4+}$ ), pentavalent ( $\text{Sb}^{5+}$ ,  $\text{V}^{5+}$ ,  $\text{Nb}^{5+}$  and  $\text{Ta}^{5+}$ ) and hexavalent ( $\text{Mo}^{6+}$ ) cations.
5. To correlate electrical properties of prepared materials and other parameters, such as composition and structure.

## REFERENCES

- Abraham, F., Boivin, J.C., Mairesse and G., Nowogrocki 1990. The BIMEVOX series: A New Family of High Performances Oxide Ion Conductors. *Solid State Ionics* 40/41: 934-937.
- Abrahams, I., Kozanecka-Szmigiel, A., and Krok, F. 2006. Correlation of defect structure and ionic conductivity in delta-phase solid solutions in the  $\text{Bi}_3\text{NbO}_7\text{-Bi}_3\text{YO}_6$  system. *Solid State Ionics* 177: 1761-1765.
- Abrahams, I., Krok, F., Chan, S.C.M., Wrobel, W., Kozanecka-Szmigiel, A., Luma, A. and Dygas, J.R. 2006. Defect structure and ionic conductivity in  $\text{Bi}_3\text{Nb}_{0.8}\text{W}_{0.2}\text{O}_{7.1}$ . *Journal of the Solid State Electrochemistry* 10: 569-574.
- Ahmadu, U., Tomas, Š, Jonah, S. A., Musa, A. O. and Rabi, N. 2013. Equivalent circuit models and analysis of impedance spectra of solid electrolyte  $\text{Na}_{0.25}\text{Li}_{0.75}\text{Zr}_2(\text{PO}_4)_3$ . *Advanced Materials Letters* 4: 185-195.
- Alga, M., Ammar, A., Essalim, R., Tanouti, B., Mauvy, F. and Decourt, R. 2005. Synthesis, sintering and electrical properties of P-doped  $\text{Bi}_4\text{V}_2\text{O}_{11}$  ceramics. *Solid State Science* 7: 1173-1179.
- Arespacochaga, N.D., Valderrama, C., Peregrina, C., Mesa, C., Bouchy, L. and Cortina, J.L. 2015. Evaluation of a pilot-scale sewage biogas powered 2.8 kW<sub>e</sub> Solid Oxide Fuel Cell: Assessment of heat-to-power ratio and influence of oxygen content. *Journal of Power Sources* 300: 325-335.
- Armstrong, R.D. and Todd, M. 1995. Interfacial electrochemistry. In *Solid State Electrochemistry*, ed. P.G. Bruce, pp 265-291. Great Britain: Cambridge University Press.
- Badwal, S.P.S. and Foger K. 1996. Solid Oxide Electrolyte Fuel Cell Review. *Ceramics International* 22: 257-65.
- Beg, S., Hafeez, S. and Al-Areqi, N.A.S. 2010. Layered  $\text{Bi}_4\text{Ba}_x\text{V}_{2-x}\text{O}_{11-(3x/2)-\delta}$ . Perovskite oxide as solid electrolyte for intermediate temperature solid oxide fuel cells. *Physica B* 405: 4370-4376.
- Borowska, C.A., Liu, X., Holdynski, M., Malys, M., Hull, S., Krok, F., Wrobel, W. and Abrahams, I. 2014. Conductivity in lead substituted bismuth yttrate fluorites. *Solid State Ionics* 254: 59-64.
- Chmielowiec, J., Paściak, G. and BujŁo, P. 2009. BIMEVOX materials for application in SOFCs. *Materials Science-Poland* 27: 1251-1256.
- Chezhina, N.V., Zhuk, N.A. and Korolev, D.A. 2016. *Journal of Solid State Chemistry* 233: 205-210.
- Cole, K. S. and Cole, R. H. 1941. Dispersion and absorption in dielectrics. *Journal of Chemical Physics* 9: 341-351.

- Doh, W.J., Keith, L.D., Matthew, A.C., Kang, T.L. and Juan, C.N. 2010. Effect of Annealing Temperature and Dopant Concentration on the Conductivity Behavior in  $(\text{DyO}_{1.5})_x\text{-(WO}_3)_y\text{-(BiO}_{1.5})_{1-x-y}$ . *Journal of the American Ceramic Society* 5: 1384-1391.
- Durmuş, S., Corumlu, V., Cifci, T., Ermis, I. and Ari, M. 2013. Electrical, structural and thermal properties of nanoceramic  $(\text{Bi}_2\text{O}_3)_{1-x-y}\text{-(Ho}_2\text{O}_3)_x\text{-(Tm}_2\text{O}_3)_y$ . *Ceramics International* 39: 5241-5246.
- Edward, M.S., Razmyar, S. and Sabolsky, K. 2012. Nano-ceria enhancement of  $\text{Bi}_2\text{Cu}_{0.1}\text{V}_{0.9}\text{O}_{5.35}$  (BICUVOX) ceramic electrolytes. *Materials Letters* 76: 47-50
- Edward, M.S., Razmyar, S. and Sabolsky, K. 2013. Microstructural, electrical, and mechanical characterization of  $\text{Bi}_2\text{Cu}_{0.1}\text{V}_{0.9}\text{O}_{5.35}$  (BICUVOX) ceramics fabricated from co-precipitation precursor powders. *Journal of Materials Science* 48: 733-743.
- Finlayson, A.P., Ward, E., Tsaneva, V.N. and Glowacki, B.A. 2005.  $\text{Bi}_2\text{O}_3\text{-WO}_3$  compounds for photocatalytic applications by solid state and viscous processing. *Journal of Power Sources* 145: 667-674.
- Fowler, R. J. 1994. *Electricity: Principle and Application*, 4<sup>th</sup> ed. New York: McGraw-Hill
- Fruth, V., Ianculescu, A., Berger, D., Preda, S., Voicu, G., Tenea, E. and Popa, M. 2006. Synthesis, structure and properties of  $\text{Bi}_2\text{O}_3$ . *Journal of the European Ceramic Society* 26: 3011-3016.
- Gadsden, J.A. (1975) *Infrared Spectra of Minerals and Related Inorganic Compounds*. Butterworth Group.
- Gal'peri, E.L., Erma, L.Y., Kolchin, I.K., Belova, M.A. and Chernyshev, K.S. 1966. Die Kristallstruktur der hochtemperatur-modifikation von wismuth(III)-oxide ( $\delta\text{-Bi}_2\text{O}_3$ ). *Zeitschrift für Anorganische und Allgemeine Chemie* 328: 44-68.
- Gattow, V. G. and Schroder, H. 1962. Die Kristallstruktur der hochtemperatur-modifikation von wismuth(III)-oxide ( $\delta\text{-Bi}_2\text{O}_3$ ). *Zeitschrift für Anorganische und Allgemeine Chemie* 328: 44-68.
- Greenblatt, M. 1994. Ionic conductors. In *Encyclopedia of Inorganic Chemistry*, ed. R. B. King, volume 3, pp. 1584-1602. New York: John Wiley and Sons.
- Guan, L.L., Le, S.R., He, S.F., Zhu, X.D., Liu, T. and Sun, K.N. 2015. Densification Behavior and Space Charge Blocking Effect of  $\text{Bi}_2\text{O}_3$  and  $\text{Gd}_2\text{O}_3$  Co-doped  $\text{CeO}_2$  as Electrolyte for Solid Oxide Fuel Cells. *Electrochimica Acta* 161: 129-136.
- Harwig, H.A. 1978. On structure of bismuth sesquioxide: The  $\alpha$ ,  $\beta$ ,  $\gamma$  and  $\delta$ -phase. *Zeitschrift für Anorganische und Allgemeine Chemie* 444: 151-166.

- Harwig, H.A. and Gerards, A.G. 1978. Electrical properties of the  $\alpha$ ,  $\beta$ ,  $\gamma$  and  $\delta$ -phase of bismuth sesquioxide. *Journal of Solid State Chemistry* 26: 265-274.
- Hervoche, C. H., Steil, M.C. and Muccillo, R. 2004. Synthesis by the polymeric precursor technique of  $\text{Bi}_2\text{Co}_{0.1}\text{V}_{0.9}\text{O}_{5.35}$  and electrical properties dependence on the crystallite size. *Solid State Science* 6: 173-177.
- Hirose, N. and West, A. R. 1996. Impedance spectroscopy of undoped  $\text{BaTiO}_3$  ceramics. *Solid State Science* 6: 164.
- Hoda, S.N. and Chang, L.L.Y. 1974. Phase Relations in the System  $\text{Bi}_2\text{O}_3$ - $\text{WO}_3$ . *Journal of the American Ceramic Society* 57: 323-326.
- Hsieh, C.Y. and Fung, K.Z. 2008. Crystal structure and electrical conductivity of cubic fluorite-based  $(\text{YO}_{1.5})_x(\text{WO}_3)_{0.15}(\text{BiO}_{1.5})_{0.85-x}$  ( $0 \leq x \leq 0.4$ ) solid solution. *Journal of Solid State Electrochemistry* 13: 951-957.
- Hsieh, C.Y., Wang, H. S. and Fung, K. Z. 2011. Effect of double doping on crystal structure and electrical conductivity of  $\text{CaO}$  and  $\text{WO}_3$ -doped  $\text{Bi}_2\text{O}_3$ . *Journal of the European Ceramic Society* 31: 3073-3079.
- Huijmas, J.P.P. 2001. Ceramics in solid oxide fuel cells. *Current Opinion in Solid State and Materials Science* 5(4): 317-323.
- Hummel, R. E. 1986. *Electronic Properties of Materials: An Introduction for Engineers*. United State: Springer-Verlag.
- Irvine, J.T.S., Sinclair, D.C. and West, A.R. 1990. Electroceramics: characterization by impedance. *Advanced Materials* 2: 132-138.
- Ishihara, T., Matsuda, H. and Takita, Y. 1994. Doped  $\text{LaGaO}_3$  perovskite type oxide as a new oxide ionic conductor. *Journal of the American Ceramic Society* 116: 3801-3803.
- Jacob, K.T., Raj, S., Rannesh, L., 2007. Vegard's law: a fundamental relation or an approximation? *International Journal of Materials Research* 9: 776-779.
- Jonscher, A. K. 1983. The measurement and interpretation of dielectric properties. *Thin Solid Film* 100: 329-334.
- Jung, D.W., Duncan, K.L., Wachsman, E.D. 2010. Effect of total dopant concentration and dopant ratio on conductivity of  $(\text{DyO}_{1.5})_x(\text{WO}_3)_y(\text{BiO}_{1.5})_{1-x-y}$ . *Acta Materialia* 58: 355-363.
- Kang, T.L., Ashley, A.L., Sang, Y.J., Gregory, T.H., Sun, J.S. and Eric, D. Wachsman. 2013. Highly functional nano-scale stabilized bismuth oxides via reverse strike co-precipitation for solid oxide fuel cells. *Journal of Materials Chemistry A* 1:6199-6207.
- Katayama, H., Tamura, S. and Imanaka, N. 2011. New bismuth ion conducting solid electrolyte. *Solis State Ionics* 192: 134-136.

- Kendall, K.R., Thomas, J.K. and Loye, H.C.Z. 1994. Oxygen ion conductivity in a new class of layered bismuth oxide. *Solid State Ionics* 70/71: 221-224
- Kharitonova, E.P., Belov, D.A., Gagor, A.B., Pietraszko, A.P., Alekseeva, O.A. and Voronkova, V.I. 2014. Polymorphism and properties of  $\text{Bi}_2\text{WO}_6$  doped with pentavalent Antimony. *Journal of Alloys and Compounds* 591: 308–314.
- Kothandapani, Z., Begum, S., Ahmad, I. Daud, I. R. and Gholizadeh, S. 2014. Study of the effect of  $\text{WO}_3$  and  $\text{Bi}_2\text{O}_3$  on the Microstructure and Electrical Properties of a  $\text{TiO}_2$  based Varistor. *Journal of Mechanical Engineering and Sciences* 6: 981-987.
- Krok, F., Abrahams, I., Wrobel, W., Chan, S.C.M., Malys, M., Bogusz, W., Dygas, J.R. 2002. Phase stability, structure and electrical conductivity in the system  $\text{Bi}_2\text{Zr}_x\text{V}_{1-x}\text{O}_{5.5-(x/2)-\delta}$ . *Solid State Ionics* 154-155: 511-516.
- Krynski, M., Wrobel, W., Mohn, C.E., Dygas, J.R., Malys, M., Krok, F. and Abrahams, I. 2014. Trapping of oxides ions in  $\delta\text{-Bi}_3\text{YO}_6$ . *Solid State Ionics* 264: 49-53.
- Leszczynska, M., Borowska-Centkowska, A., Malys, M., Dygas, J.R., Krok, F., Wrobel, W. and Abrahams, I. 2015. The double rare-earth substituted bismuth oxide system  $\text{Bi}_3\text{Y}_{1-x}\text{Yb}_x\text{O}_6$ . *Solid State Ionics* 269: 37-43.
- Levin, E. M. and Roth, R. S. 1964. Polymorphism of bismuth sesquioxide. II. Effect of oxide additions on the polymorphism of  $\text{Bi}_2\text{O}_3$ . *Journal of Research of the National Bureau of Standards-A* 68A: 189-206.
- Levinson, L.M. 1987. Recent advances in piezoelectric ceramics. In *Electronic Ceramics- Properties, Devices and Applications*, ed. M.O. Thurston, and W. Middendorf, pp 45-147. New York: Marcel Dekker, Inc.
- Li, Z.B., Ding, D., Liu, M.F., Ding, X.F., Chen, D.C., Li, X.X., Xia, C.R. and Liu, M.L. 2013. High-performance, ceria-based solid oxide fuel cells fabricated at low temperatures. *Journal of the Power Sources* 241: 454-459.
- Lin, S.E. and Wei, W.C.J. 2011. Long-term degradation of  $\text{Ta}_2\text{O}_5$ -doped  $\text{Bi}_2\text{O}_3$  systems. *Journal of the European Ceramic Society* 31: 3081-3086.
- Ling, C.D. 1999. Structural relations among bismuth-rich phases in the  $\text{Bi}_2\text{O}_3\text{-Nb}_2\text{O}_3$ ,  $\text{Bi}_2\text{O}_3\text{-Ta}_2\text{O}_3$ ,  $\text{Bi}_2\text{O}_3\text{-MoO}_3$  and  $\text{Bi}_2\text{O}_3\text{-WO}_3$  Systems. *Journal of Solid State Chemistry* 148: 380-405.
- Ma, H.Q., Lin, K., Fan, L.L., Rong, Y.C., Chen, J., Deng, J.X., Liu, L.J., Kawaguchi, S., Kato, K.C. and Xing, X.R. 2015. Structure and oxide ion conductivity in tetragonal tungsten bronze  $\text{BaBiNb}_5\text{O}_{15}$ . *The Royal Society of Chemistry Advances* 71890-71895.
- Mączka, M., Fuentes, A.F., Kępiński, L., Diaz-Guillen, M.R., Hanuza, J. 2010. Synthesis and electrical, optical and phonon properties of nanosized Aurivillius  $\text{Bi}_2\text{WO}_6$ . *Materials Chemistry and Physics* 120:289-295.

- Mahato, N., Banerjee, A., Gupta, A., Omar, S. and Balani, K. 2015. Progress in material selection for solid oxide fuel cell technology. *Progress in Materials Science* 72: 141-337.
- Mairesse, G. 1993. *In fast ion transport in solids*, ed. B. Scrosati, Amsterdam: Kluver.
- Malys, M., Abrahams, I., Krok, F., Wrobel, W. and Dygas, J.R. 2008. The appearance of an orthorhombic BIMEVOX phase in the system  $\text{Bi}_2\text{Mg}_x\text{O}_{5.5-3x/2-\delta}$  at high values of x. *Solid State Ionics* 179: 82-87.
- Michihiro, Y., Itabashi, A., Yamanishi, T., Kanashiro, T., Kishimoto, Y. and Iwahara, H. 1994. Complex Impedance Study in  $\text{Bi}_2\text{O}_3\text{-WO}_3$ . *Journal of the Physical Society of Japan* 63: 4456-4462.
- Moos, R., Menesklou, W., Schreiner, H.J. and Härdtl, K.H. 2000. Materials for temperature independent resistive oxygen sensors for combustion exhaust gas control *Sensors and Actuators B* 67: 178-183.
- Morozova, M.V., Buyanova, E.S., Emelyanova, Y.V., Zhukovskiy, V.M., Petrova, S.A., Zakharov, R.G. and Tarakina, N.V. 2011. Specific features in the synthesis, crystal structure and electrical conductivity of BICUTIVOX. *Solid State Ionics* 201: 27-34.
- Moulson, A. J. and Herbert, J. M. 2003. *Electroceramics*, ed. A.J. Moulson and J.M. Herbert, pp 1-5. England: John Wiley & Son Ltd.
- Nespolo, M., Watanabe, A. and Suetsugu, Y. 2002. Re-investigation of the structure of  $7\text{Bi}_2\text{O}_3\cdot 2\text{WO}_3$  by single-crystal X-ray diffraction. *Crystal Research and Technology* 37: 414-422.
- Niu, Y.J., Sunarso, J., Zhou, W., Liang, F.L., Ge, L., Zhu, Z.H. and Shao, Z.P. 2011. Evaluation and optimization of  $\text{Bi}_{1-x}\text{Sr}_x\text{FeO}_{3-\delta}$  perovskites as cathodes of solid oxide fuel cells. *International Journal of Hydrogen Energy* 36: 3179-3186.
- Payne, J.L., James, D.F., Alistair, M.L., Mark, R.J., Ivana, R.J. and Ivana, R.E. 2013. The mechanism of oxide ion conductivity in bismuth rhenium oxide,  $\text{Bi}_{28}\text{Re}_2\text{O}_{49}$ . *Solid State Ionics* 244: 35-39.
- Pelosato, R., Cordaro, G., Stucchi, D., Cristiani, C. and Dotelli, G. 2015. Cobalt based layered perovskites as cathode material for intermediate temperature Solid Oxide Fuel Cells: A brief. *Journal of Power Sources* 298: 46-67.
- Pereira, G.J., Castro, R.H.R., De Florio, D.Z., Muccillo, E.N.S. and Gouvêa, D. 2005. Densification and electrical conductivity of fast fired manganese-doped ceria ceramics. *Materials Letters* 59: 1195-1199.
- Piva, R.H., Piva, D.H., Venturini, J., Floriano, R. and Morelli, M.R. 2015. Inhibition of order-disorder phase transition and improvements in the BICUVOX.1 properties by using yttria-stabilized zirconia particles. *Ceramics International* 41: 171-177.

- Raghvendra, S.R.K. and Singh, P. 2014. Synthesis of  $\text{La}_{0.9}\text{Sr}_{0.1}\text{Ga}_{0.8}\text{Mg}_{0.2}\text{O}_{3-\delta}$  electrolyte via ethylene glycol route and its characterizations for IT-SOFC. *Ceramics International* 40: 7177-7184.
- Raghvendra and Singh, P. 2015. Influence of  $\text{Bi}_2\text{O}_3$  additive on the electrical conductivity of calcia stabilized zirconia solid electrolyte. *Journal of the European Ceramic Society* 35: 1485-1493.
- Rahaman, M.N. 2003. *Ceramic Processing and Sintering*, second edition, Taylor & Francis Group, CRC Press.
- Sammes, N. M., Tompsett, G. A., Näfe, H. and Aldinger, F. 1999. Phase transitions and electrical properties of bismuth sesquioxide. *Journal of Physical Chemistry* 73: 672-675.
- Sekiya, T., Mochida, N., Ogawa, S.J. 1994. Structural study of  $\text{WO}_3\text{-TeO}_2$  glasses. *Journal of non-crystalline solids* 176: 105-115.
- Shaikh, S.P.S., Muchtar, A. and Somalu, M.R. 2015. A review on the selection of anode materials for solid-oxide fuel cells. *Renewable and Sustainable Energy Reviews* 51: 1-8.
- Shao, Z.P., Zhou, W. and Zhu, Z.H. 2012. Advanced synthesis of materials for intermediate-temperature solid oxide fuel cells. *Progress in Materials Science* 57: 804-874.
- Sharma, V., Shukla, A.K. and Gopalakrishnan 1992. Effect of aliovalent-cation substitution on the oxygen-ion conductivity of  $\text{Bi}_4\text{V}_2\text{O}_{11}$ . *Solid State Ionics* 58: 359-362.
- Shuk, P. and Mobius, H. H. 1985. Oxide-ion conducting electrolytes. 40. Transport numbers and electrical conductivity of modifications of bismuth (III) oxide. *Zeitschrift fuer Physikalische Chemie* 266: 9-16.
- Shuk, P., Wiemhöfer, H.D., Guth, U., Göpel, W. and Greenblatt, M. 1996. Oxide ion conducting solid electrolytes based on  $\text{Bi}_2\text{O}_3$ . *Solid State Ionic* 89: 179-196.
- Sinclair, D.C., Morrison, F.B. and West, A.R. 2000. Applications of combined impedance and electric spectroscopy to characterise electroceramics. *Ceramic International* 2: 33-38.
- Speranskaya, E.I. 1970. The Bismuth Oxide-Tungsten Trioxide System. *ZInorganic Mater* 6: 127-129.
- Steele, B.C.H. 1991. Electronic Ceramics. In *Electronic Ceramics*, ed. B.C.H. Steele, pp 1-5. New York: Academic Press, Inc.
- Steele, B.C.H. 2000. Appraisal of  $\text{Ce}_{1-y}\text{Gd}_y\text{O}_{2-y/2}$  electrolytes for ITSOFC operation at 500 °C. *Solid State Ionics* 129: 95-110.

- Steil, M.C., Fouletier, J., Kleitz, M. and Labrune, P. 1999. BICOVOX: Sintering and Grain Size Dependence of the Electrical Properties. *Journal of the European Ceramics Society* 19: 815-818.
- Smolyaninov, N. P. and Belyaev, I. N. 1962. Investigation of the System  $\text{Bi}_2\text{O}_3\text{-WO}_3\text{-PbO}$ . *Russian Journal of Inorganic Chemistry* 7: 1345-1348.
- Takahashi, T. and Iwahara, H. 1973. High oxide ion conduction in sintered oxides of the system  $\text{Bi}_2\text{O}_3\text{-WO}_3$ . *Journal of Applied Electrochemistry* 3: 65-72.
- Takahashi, T. and Iwahara, H. 1978. Oxide ion conductors based on bismuth sesquioxide. *Material Research Bulletin* 13: 1447-1453.
- Takahashi, T., Iwahara, H. and Nagai, Y. 1972. High oxide-ion conductivity in sintered  $\text{Bi}_2\text{O}_3$  containing  $\text{SrO}$ ,  $\text{CaO}$  or  $\text{La}_2\text{O}_3$ . *Journal of Applied Electrochemistry* 2: 97-104.
- Taninouchi, Y.K., Uda, T., Ichitsubo, T., Awakura, Y. and Matsubara, E., 2010. High oxide-ion conductivity of monovalent-metal doped bismuth vanadate at intermediate temperatures. *Solid State Ionics* 181: 719-723.
- Taoufyq, A., Ahsaine H. A., Patout, L., Benlhachemi, A., Ezahri, M., Guinneton, F., Lyoussi, A., Nolibe, G. and Gavarrri, J.R. 2014. Electron microscopy analyses and electrical properties of the layered  $\text{Bi}_2\text{WO}_6$  phase. *Journal of Solid State Chemistry* 203: 8-18.
- Tukamoto, H. and West, A. R. 1997. Electronic conductivity of  $\text{LiCoO}_2$  and its enhancement by magnesium doping. *Journal of the Electrochemical Society* 144(9): 3164-3168.
- Watanabe, A. 1995. Preparation of a new phase having a cation-ordered c-type rare-earth oxide related structure in the systems  $\text{Bi}_2\text{O}_3\text{-Ln}_2\text{O}_3$  ( $\text{Ln} = \text{Sm}, \text{Eu}, \text{Gd}, \text{Tb}, \text{and Dy}$ ). *Journal of Solid State Chemistry* 120(1): 32-37.
- Watanabe, A., Ishizawa, N. and Kato, M. 1985. An Outline of the Structure of  $7\text{Bi}_2\text{O}_3\cdot 2\text{WO}_3$  and Its Solid Solution. *Journal Solid State Chemistry* 60:252-257.
- Watanabe, A. and Ono, A. 2004. Thermostable region of an oxide ion conductor,  $\text{Bi}_7\text{WO}_{13.5}$  ( $=7\text{Bi}_2\text{O}_3\cdot 2\text{WO}_3$ ) and the solid solubility extension. *Solid State Ionics* 174: 15-18.
- Watanabe, A. and Sekita, M. 2005. Stabilized  $\delta\text{-Bi}_2\text{O}_3$  phase in the system  $\text{Bi}_2\text{O}_3\text{-Er}_2\text{O}_3\text{-WO}_3$  and its oxide-ion conduction. *Solid State Ionics* 176: 2423-2428.
- West, A.R. 1999. *Basic Solid State Chemistry*, 2<sup>nd</sup> ed. Chichester: John Wiley and Sons.
- Xu, Y.L., Zhou, X.H. and Sorensen, O.T. 2000. Oxygen sensors based on semiconducting metal oxides: an overview. *Sensors and Actuators B* 65: 2-4.

Yan, J. and Greenblatt, M. 1995. Ionic conductivities of  $\text{Bi}_4\text{V}_{2-x}\text{M}_x\text{O}_{11-x/2}$  (M = Ti, Zr, Sn, Pb) solid solutions. Oxygen sensors based on semiconducting metal oxides: an overview. *Solid State Ionics* 81: 225-233.

Yamada, T. 2003. Ionic conductor oxygen sensor. In *Handbook of Advanced Ceramics*, pp 37-58.

